NTNU – Trondheim
Norwegian University of
Science and Technology

The Relative Influence of Solar Radiative and Solar Geomagnetic Variation on the Dynamics of the Polar Upper Mesosphere

Randi Synnøve Hegdal Chapana

Master of Science in Physics and Mathematics
Submission date: June 2012
Supervisor: Robert Edward Hibbins, IFY

Norwegian University of Science and Technology
Department of Physics

The Relative Influence of Solar Radiative and Solar Geomagnetic Variation on the Dynamics of the Polar Upper Mesosphere

Randi Synnøve Hegdal Chapana
Department of physics, NTNU, N-7491 Trondheim, Norge

Academic supervisor: Robert Edward Hibbins

June 15, 2012

Problem Description

In this thesis, mesospheric wind will be compared with the global *Ap* index measuring the perturbation of the geomagnetic field on earth, along with the measure for solar radiance, the *F10.7* index. Hourly wind data from the SuperDARN radars Goose Bay, Hankasalmi, Kapuskasing, King Salmon, Kodiak, Pykkvibær, Saskatoon and Stokkseyri in the northern hemisphere and monthly geomagnetic and solar irradiance data from the web page of the U.S. Dept. of Commerce, NOAA, Space Weather Prediction Center (SWPC) will be used.

Sammendrag på Norsk

Nyere forskning viser at det kan være en sammenheng mellom forstyrrelser i jordens magnetfelt grunnet solvind, og sirkulasjonen i atmosfæren. Disse effektene vil være lettere å finne i mesosfæren enn i lavere deler av atmosfæren. Mesosfæren er ikke så tilgjengelig som den lavere atmosfæren, og få har undersøkt bølgebevegelse her. Meridional og sonal vind i mesosfæren, fra SuperDARN radarene Goose Bay, Hankasalmi, Kapuskasing, King Salmon, Kodiak, Pykkvibær, Saskatoon and Stokkseyri i den nordlige hemisfæren, ble sammenlignet med den globale *Ap* indeksen og *F10.7* indeksen som er målet på sol irradians. Vinddata fra SuperDARN radarene var tilgjengelig for hver time, mens geomagnetisk data og data for sol irradiansen var tilgjengelig for hver måned. Periodiske variasjoner ble fjernet fra vinddataene og forskjellen i vind mellom høy og lav *Ap* og *F10.7* ble brukt for å se om man kunne finne en sammenheng mellom de to indeksene og vinden i mesosfæren, og om de påvirket vinden på en lignende måte. En tendens til østlig vind og vind mot ekvator ble funnet i perioder med høy geomagnetisk aktivitet. I tillegg øker effekten med økende geomagnetisk breddegrad for den sonale vinden. *Ap* og *F10.7* påvirket ofte vinden på lignende måter og det var vanskelig å skille dem fra hverandre. Korrelasjonen mellom disse viste seg å være høy når lineær regresjon ble brukt for samme tidsramme som i denne oppgaven.

Preface

This is a master thesis written during the spring semester of 2012 at NTNU, department of physics. It is a continuation of the master project written in autumn 2011. I would like to thank my supervisor, professor Robert Hibbins for informative explanations and helpful guidance along the way in addition to correcting my English. I would also like to give thanks to Alan and Damian for being patient and supportive and to my parents for supporting both with words and practical help. At last, thanks to Eva Mørtsell for proof reading my thesis.

Trondheim June, 2012

Randi Synnøve Hegdal Chapana

Abstract

Resent research indicates that there might be a connection between perturbation of the Earth's geomagnetic field caused by solar wind, and the atmospheric circulation. In this project the mesospheric meridional and zonal wind, obtained from the SuperDARN radars Goose Bay, Hankasalmi, Kapuskasing, King Salmon, Kodiak, Pykkvibær, Saskatoon and Stokkseyri in the northern hemisphere was compared with the global *Ap* index along with the measure for solar radiance, the *F10.7* index. Wind data from the SuperDARN radars were available for every hour and geomagnetic and irradiance data for every month. The solar atmospheric tides along with seasonal effects were removed from the wind data and the perturbation of the residual wind due to *Ap* and *F10.7* was used to see if any connection between the mesospheric wind and *Ap*/*F10.7* could be found, and if they influenced the wind in a similar manner. A tendency for more equatorwards and eastwards winds during periods of high geomagnetic activity was found. In addition, this effect was observed to increase with increasing geomagnetic latitude for the zonal wind. *Ap* and *F10.7* often affected the wind in a similar manner, making it hard to distinguish the two. Using linear regression, the correlation between them was found to be high over the timescales of this study.

Contents

1 Introduction

In order to understand how man made changes in the atmosphere affect the climate, it is crucial to understand the natural changes. In the mesosphere, planetary waves, gravity waves and solar atmospheric tides are found. As waves rise through the atmosphere, the density decreases causing the wave amplitudes to increase. At last they break, depositing momentum. Zonal gravity waves propagating in the opposite direction to the background wind are filtered through the stratosphere and into the mesosphere. This creates a summer to winter hemisphere flow, with zonal wind mainly present through the coriolis effect.

It is well known that the Sun affects the climate on Earth through radiation, often measured by the *F10.7* index, but there is evidence that it might also affect the climate through influencing the circulation of the atmosphere by indirect sources such as solar particles flowing into the Earth's ionosphere. This effect is measured by the *Ap* index which shows the general geomagnetic activity over the globe.

Lu et al., 2008 [15] reported both an increase in temperature and more westward wind in the stratosphere with increasing *Ap* values. Chang et al., 2009 [6] found the same periodicity in mesosphere and lower thermosphere (MLT) temperature as is known to exist in solar wind, namely a 9 day periodicity. Both articles mention EPP as a possible cause to this effect. The contribution of EPP to creation of nitric oxide (NO) has been confirmed by Daae et al., 2011 [7], and Newnham et al., 2011 [21]. Both found increased levels of NO and depletion of ozone directly after small geomagnetic storms.

In this thesis, mesospheric meridional and zonal wind will be compared with the geomagnetic *Ap* index and the *F10.7* index to see if any connection can be found. Hourly wind data from the SuperDARN radars Goose Bay, Hankasalmi, Kapuskasing, King Salmon, Kodiak, Pykkvibær, Saskatoon and Stokkseyri, [30] in the northern hemisphere (NH) and monthly geomagnetic data from the web page of the U.S. Dept. of Commerce, NOAA, Space Weather Prediction Center (SWPC) [33] are used. Hourly residual wind data with the tidal climatology for each month subtracted, are fitted to sinusoids representing the solar atmospheric tidal waves, and the monthly mean residual wind from this fit is used for comparison with the *Ap* and *F10.7* data. The correlation between *Ap*/*F10.7* and the monthly mean wind is then investigated. Next, the perturbation of the monthly mean residual wind from *Ap*/*F10.7* is used to find how the mesospheric wind is connected to *Ap*/*F10.7* and if the indexes affect the wind in a similar way.

The text first goes through some theory about the atmosphere and its circulation along with theory about the Sun and how it affects the atmosphere. Next, previous work on the topic is mentioned, as this is important for the initiation of the project. The next section contains a description of the data followed by an explanation of how the data were handled. Finally results are presented and discussed.

2 Theory

The lower to middle atmosphere is divided into the troposphere, stratosphere and mesosphere as seen in figure 1. In the troposphere, most of the observed weather phenomena such as cloud formation, hurricanes and thunderstorms take place. In the lower stratosphere, the part of the atmosphere with the highest concentration of ozone (O_3), called the ozone layer, is found. The altitude for the different layers changes with latitude and season. [1]

The mesosphere and lower thermosphere are called the MLT region. Here, the air density is very low and waves propagating into this region have big amplitudes. Waves found here are planetary waves, gravity waves and solar atmospheric tides propagating upward from lower levels of the atmosphere. [6] These dissipate in the MLT by turbulent eddies, or increasing molecular diffusion in the lower thermosphere. [25]

In the atmosphere there are many different types of oscillations and periodical waves, such as the solar atmospheric tides, the planetary waves and the gravity waves. These waves allow the entire atmosphere to be connected if not through direct movement of mass, then through propagation of momentum and temperature.

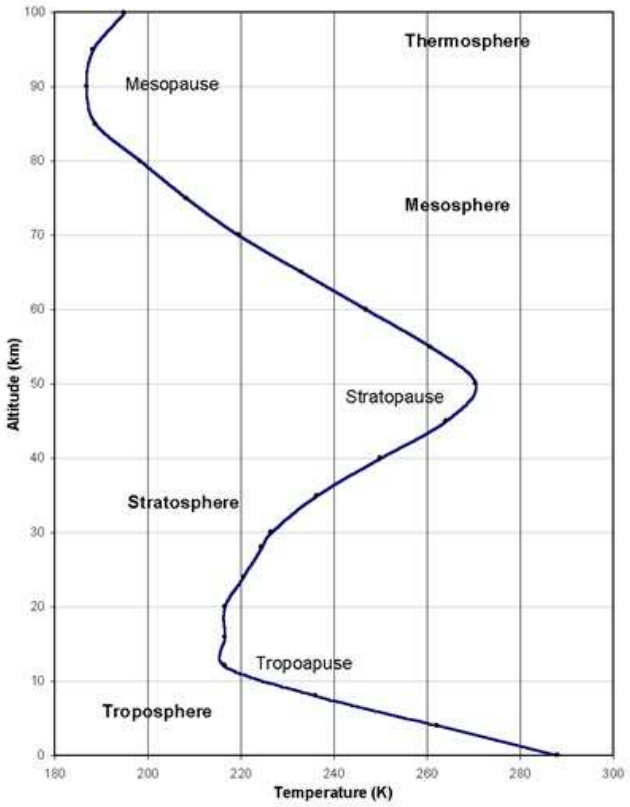

Figure 1: The Earth's temperature profile as a function of height (US Standard Atmosphere, 1976) [36].

2.1 Planetary Waves

Planetary waves propagate because of how the coriolis effect varies with latitude. The coriolis effect is due to the Earth's rotation and deflects a portion of air to move to the right of its motion in the northern hemisphere (NH) and to the left in the southern hemisphere (SH). The planetary waves are dependent upon the rotation and spherical geometry of the Earth. In addition they are forced partly by land-sea contrasts and surface topography. The planetary waves can have horizontal scales of thousands of kilometers and periods of several days. Some planetary waves are stationary, i.e. from a point on Earth it seems that they do not move, however they can still propagate information as they are dispersive i.e. their group velocity and phase velocity can be in different directions. Other planetary waves move with respect to the Earth. The wave crests and troughs, moving with the phase speed, usually move westward with respect to the background flow. The group velocity, however, can be in any direction. Stationary waves only propagate vertically in eastward background flow. Moreover, waves with longer wavelengths can propagate in stronger background flows than shorter wavelengths. This means that more waves with longer wavelengths are able to propagate than the ones with shorter wavelengths. This effect is seen in the NH winter stratosphere where the background wind is eastward and stationary planetary waves have long wavelengths propagating vertically and meridionally into the winter stratosphere. In contrast, the summer stratosphere, with westward wind, has no stationary planetary waves. [1]

The planetary waves form in the troposphere around the equator and propagate upward into the stratosphere and towards the poles. Here they break and deposit momentum, driving the stratospheric Brewer-Dobson circulation.

As the NH has much greater land-sea contrast and larger mountain ranges than the SH, larger amplitude planetary waves are created here. The NH therefore has much stronger planetary wave activity. The stratospheric polar winds vary with season. In winter, the zonal wind is eastward, while in summer the wind is westward. This effect is however not seen in the troposphere to such an extent. Even in midwinter, large amplitude planetary waves moving westward on the eastward background wind, can change the wind in the NH polar area from eastward to westward, leading to a dramatic warming of the stratosphere. These events are called major stratospheric warmings and only occur in years when the planetary wave amplitudes are large enough to change the wind from eastward to westward. [3]

2.2 Gravity Waves

The gravity waves are fluid dynamical waves that form throughout the atmosphere where the fluid pressure, density, temperature and velocity fluctuate together. Some gravity waves form near the ground, for instance when air passes over a mountain. The air is pushed over the obstacle and is lead into a sinusoidal like movement. These can propagate up into the stratosphere or mesosphere. Other gravity waves form further up in the atmosphere i.e. by convective activity in the troposphere. Gravity waves are dispersive, if the phase surface moves downward, the propagation of information through the group velocity happens upward. In addition, the ampli-

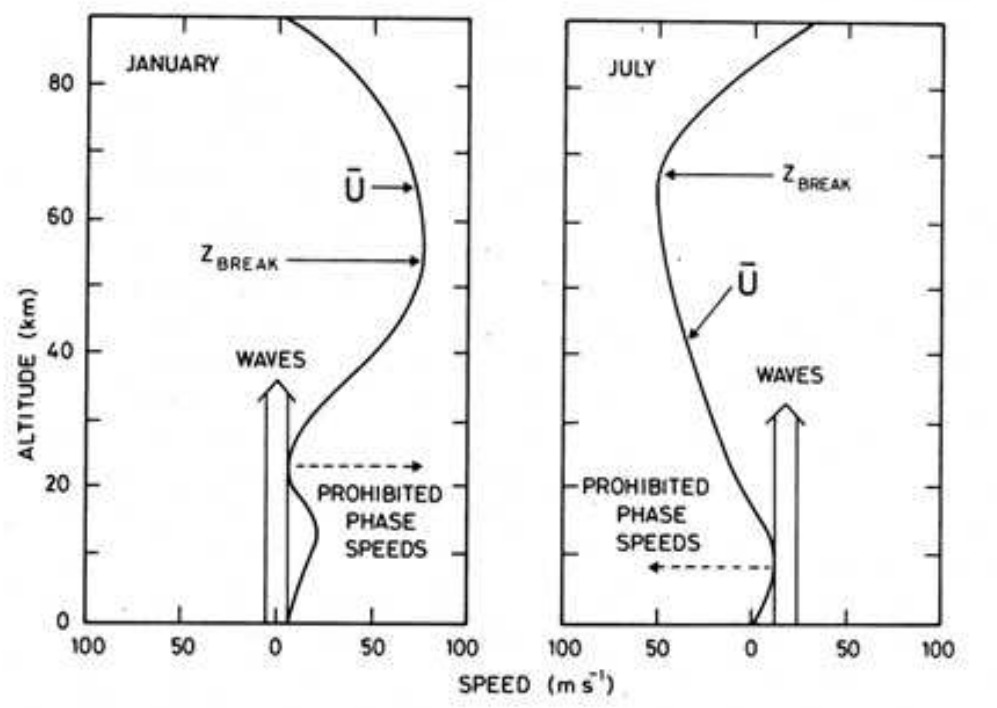

Figure 2: Zonal wind as a function of height in NH winter and summer. The approximate breaking levels and permitted phase speeds of upward propagating gravity waves are also shown. [5]

tudes of the wave fluctuations in the wind increase along with the amplitudes of the fluctuations in temperature and density, as the density of the air decreases. If they reach the mesosphere, the gravity waves dissipate or break and deposit momentum. Consequently the gravity waves in the mesosphere can influence the atmosphere here substantially. [1]

There is a big difference in solar heat entering the atmosphere with most heat entering the equatorial area, due to a $\cos\theta$ difference with latitude. Variations in Earth inclination and Earth-Sun distance also influence this. As the energy output from the Earth does not have as big variations over latitudes, the energy is transported poleward. This gives a strong latitudinal gradient in winter, driving strong meridional winds. Due to the deflection of the waves by the coriolis force, this also creates zonal winds. The poleward wind is deflected eastward, and wind from the pole is deflected westward. This is the main driver of the global circulation in the troposphere. [8]

In summer the eastward propagating gravity waves are let through the westward winds in the stratosphere to enter the mesosphere, while in winter, westward propagating gravity waves are let through the stratospheric eastward winds as shown in figure 2. This effect therefore decelerates the wind in the mesosphere in both the summer and winter hemispheres, making the winds go from summer to winter hemispheres. This also creates a zonal wind through the coriolis effect. In the summer hemisphere the mesospheric air rises and is cooled, while in the winter hemisphere the air is compressed and heated. [8, 10]

2.3 Solar atmospheric Tides

In the mesosphere, the tidal waves can dominate the wind field due to their large amplitudes. They also transfer momentum and affect the circulation of the atmosphere.[4] The tidal waves appear due to the Sun warming the atmosphere at day time and not at night. The different tidal modes are the atmospheric response to this forcing. They can have a 24 hour component called the diurnal tide and a 12 hour component called the semidiurnal tide. It can also have an 8 and 6 hour component, but these have smaller amplitudes. If the 24, 12 and 8 hour components are included, the sinusoidal looks like this:

$$W = A_{24}\sin(\frac{2\pi k}{24} - \phi_{24}) + A_{12}\sin(\frac{4\pi k}{24} - \phi_{12})) + A_8\sin(\frac{6\pi k}{24} - \phi_8) \qquad (1)$$

Where A_i is the amplitude of the i'th hour component and ϕ_i is the phase displacement of the i'th hour component where $i = 24, 12, 8$.

2.4 The solar Cycle

During an 11 year cycle the number of sunspots on the surface of the Sun decrease and increase. The cycle has varied in length from eight to fourteen years, indicating that the length of the cycle is not constant. As the number of sunspots increase, so does the solar activity leading to solar flares and coronal mass ejections (CMEs) releasing high amounts of radiation and solar material. The solar minimum is defined as when the Sun has the least sunspots in a cycle and maximum when it has the most. The intensity for each cycle can however vary significantly. There is a shifting of north and south pole in the Sun which happens every 11 years, causing the increase and decrease in number the of sunspots. The shift is driven by the differential rotation of the magnetic material inside the Sun causing stretching and twisting and at last leading to a total shift of the poles. At the beginning of a solar cycle, with increasing number of sunspots, the sunspots appear at mid latitudes at each side of the equator of the Sun. As the solar cycle proceeds, the sunspots move further towards the equator. This is often shown in a butterfly diagram as in figure 3. As the sunspots are colder than the surrounding surface of the Sun, they appear darker. [18, 19]

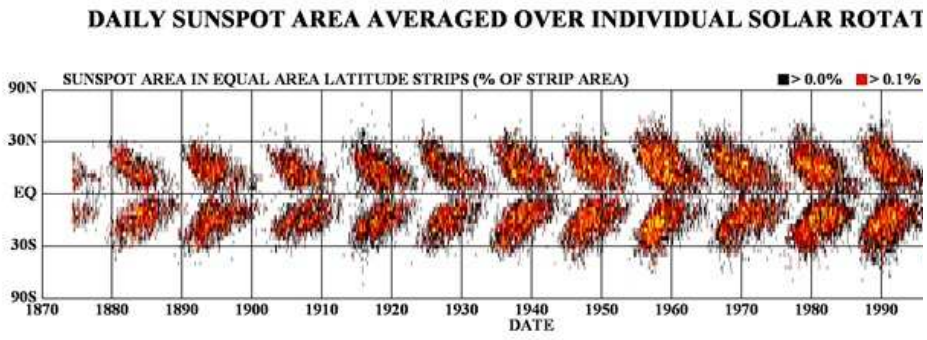

Figure 3: A butterfly diagram showing how the sunspots move over the solar hemispheres during several solar cycles.[18]

2.5 Solar Irradiance

The Sun emits electromagnetic radiation in wavelengths from 0.01 nm to more than 100 m. The Earth is however protected by the atmosphere from most frequencies due to absorption by the gases in the atmosphere at certain wavelengths. The wavelengths where the electromagnetic waves are not absorbed are called atmospheric windows. Such windows exist for visible light at 300 - 750 nm, some in infrared from 1 - 13 μm and for radio waves from 1 cm to 30 m. [37]

The total radiant energy over all wavelengths received by the Earth from the Sun measured outside Earth's atmosphere is called the total solar irradiance (TSI). This was once assumed to be constant, but as soon as this could be measured by satellite instruments, the assumption was proven erroneous. The total solar irradiance mainly varies with the 11 year solar cycle, but also has longer and shorter term variability. When big sunspots pass over the disc of the Sun facing Earth, a decrease in the total irradiance up to 0.34 percent has been recorded [20]. Still the total irradiance increases with solar cycle maximum when the number of sunspots is high. This was a mystery until the faculae were discovered. The faculae are bright, warmer spots on the Sun accompanying the sunspots. As the sunspots increase in number during a solar cycle, so do the faculae to the point where they brighten the Sun more than the sunspots dim it at the solar maximum. [17, 20]

The F10.7 index is an often used as a measure for the total solar irradiance reaching Earth because it acts as a proxy for all wavelengths and is easy to observe. The F10.7 index is discussed further in section 4.3.

2.6 Perturbation of the geomagnetic Field

The Earth is constantly hit by solar wind with velocity between 200 and 700 km/s, containing mainly protons and electrons along with α particles and heavier ions. The stream of plasma also brings along a magnetic field from the Sun, called the interplanetary magnetic field. Bigger energy releases from the surface of the Sun, called flares can release up to 10^{32} ergs/s = 10^{25} J. [26]. There are more flares when the Sun is active, i.e. has many sunspots, than when it is quiet, following the 11 year solar cycle. The high temperature solar flares emit radiation mostly in the extreme ultra violet (EUV) region, ranging from 10 to 120 nm, in the x-ray region, ranging from 0.01 to 10 nm and in the radio wave region, ranging from 1 mm to 100 km. Flares observed in the visible part of the electromagnetic spectrum are called low temperature flares. The flares are believed to be created by twisting of the magnetic field in the sunspots until the stored magnetic energy is converted into thermal and kinetic energy and is released as a flare.

Another high energy outburst from the Sun is the coronal mass ejection (CME). In contrast to the solar flares that at times produce most thermal energy, the energy of the CME is mostly kinetic. These events are not as frequent as solar flares and vary from 1-6 events through the 11 year solar cycle. [26] Flares and CME can cause geomagnetic storms in the Earth's magnetosphere which interact with the Earth's magnetic field. This causes an increase in particles that enter through the Earth's magnetosphere precipitating down into the MLT region. The more energetic the particles, the further down they precipitate. [15]

2.7 Geomagnetic Coordinates

The radiation received from the Sun at one location on Earth varies through the day, season and year. At the equator the radiance is greatest while the poles receive less. The incoming radiance over the poles depends on how the Earth is tilted. To measure how the wind in the polar areas respond to solar irradiance it would therefore be natural to use geographic coordinates centered at the rotational axis of the Earth.

The particles entering the Earth atmosphere from the Sun, is of a more constant rate where day and night and seasonal variation does not matter as much. These particles bombard the magnetic field all over Earth, but only enter around the geomagnetic poles where the magnetic field lines are vertical. So when measuring how solar particles affect the atmosphere, the geomagnetic coordinates are more natural to use.

The geomagnetic poles are computed from a geomagnetic model. According to the World Magnetic Model (WMM) the geomagnetic north pole had the coordinates: 72.21°W longitude and 80.08°N latitude in geographic coordinates as of 2010. Since the first detection, the magnetic north pole has moved at an increasing rate, and is now moving at a rate of 50 km per year. The geomagnetic poles are the center for the auroral oval. The auroral oval is a 5° latitude band around the geomagnetic poles occurring as far as 15° to 25° away from the poles when the solar activity is high. [22] [16]

3 Previous Evidence of *Ap* induced Changes in the Atmosphere

Arnold and Robinson, 2001 [2] used a model to see if changes in the thermosphere by the high energy particles from the solar wind could be traced in the winter stratosphere. They found that it was not probable that the changes in geomagnetic activity affected the stratosphere directly, but rather indirectly by propagation of information by the planetary waves. In summer the propagation of planetary waves is blocked by westward flow conditions and coupling between the thermosphere and stratosphere was small.

Lu et al.,2007 [14] found an increase in temperature deviation of 0.1-0.7 K due to geomagnetic activity in the equatorial regions in the stratosphere. The *Ap* signals were strengthened when the quasi-biennial oscillation (QBO) was westerly or solar irradiance was high. To continue, Lu et al., 2008 [15] studied formation of NO_x by energetic particle precipitation (EPP-NO_x) in the upper mesosphere and thermosphere and how it affected the stratospheric wind and temperature in late winter and spring. They found downward propagating geomagnetic signals in the polar regions of both hemispheres in spring when years of sudden stratospheric warming were removed from the data. They also found that when the *Ap* index was high, the wind was more westward in both hemispheres, and the temperature was warmer. It was suggested that the *Ap* influence on the stratosphere was not by the direct effect of EPP-NOx, but indirectly perhaps by propagating the changes made further up in the atmosphere downward with waves as suggested by Arnold and Robinson, 2001 [2]. The details in this propagation of the *Ap* signals was undetermined.

It is known that the solar wind has periodicities of 9, 7 and 5.5 days giving the same periodicity in the *Ap* index [31, 12]. Thayer et al., 2008 [31] found a statistically significant 9 day periodicity in infrared data and the *Ap* index while Lei et al.,2008a,b [12, 13] found a 9 day solar period in density variations in the Earth's thermosphere. Chang et al., 2009 [6] discovered a correlation between temperature changes in the MLT and geomagnetic perturbation with periods of solar rotation sub harmonics. Zonally symmetric modulation in the temperature with a period of 9 days was found below 120 km. They found that this relation was confined to latitudes polewards of 40^o. More towards the equator than this, the correlation was not significant. The coverage of SABER satellite data was poor above 50^o so the effect in the polar areas could not be investigated with these data, but at 75^o, using lower quality data, stronger effects were detected. It was not excluded that this result came from EPP as investigated by Lu et al. [2008] since these effects also peak near 110 km altitude.

A near connection between precipitating particles from a weak coronal mass ejection (CME)and NO production in the mesosphere has been found by Daae et al., 2011 [7] in the SH. Electrons precipitating down to 70 km height due to a moderate geomagnetic storm caused by a CME, generated a significant NO increase in the middle mesosphere. An increase in OH temperature at 87 km by 10-20 degrees was also observed. Following, an immediate 30% depletion of O_3 at altitude 62 to

80 km was also seen. This descended down to 55 km with velocity 1-3 cm/s and an O_3 depletion was found from 55 to 80 km for 9 days.

A similar result has been reported by Newnham et al., 2011 [21]. They found enhanced levels of NO which lasted 3-4 days in the SH during small geomagnetic storms. The volume mixing ratio increased by 2-3 orders of magnitude above normal, reaching levels of 1.2 ppmv. They also found that the NO has been produced directly in the mesosphere through electron precipitation. These results show that even moderate geomagnetic storms that also occur during solar minima can induce traceable changes in the chemistry of the atmosphere potentially affecting its circulation.

Singer et al., 1994 [28] investigated the influence of geomagnetic storms on the MLT region, using two MF radars, four meteor radars and two LF wind profilers at middle geomagnetic latitudes (50-55^{o}N) and high geomagnetic latitudes (60.5^{o}N) in the NH. They found enhanced westward directed winds when *Ap* was high, at middle geomagnetic latitudes and enhanced eastward directed winds when *Ap* was high, at high geomagnetic latitudes. A weaker effect was found in the meridional wind than in the zonal wind. The results were however of poor statistical quality.

Keuer et al., 2007, [11] using the solar Lyman α values, which are closely correlated to the *F10.7* index, found increasing eastward wind in summer and increasing westward wind in winter with increasing solar radiance for height above 83 km in the NH. Below this height, the trend was opposite. The meridional wind moved more southward both in summer and winter when the solar Lyman α was high. This for heights above 85 km. Below this height, the wind perturbation was northward in summer and near zero in winter. The measurements were done at 54.6^{o}N and 13.4^{o}E between 1990 and 2005.

Pancheva et al., 2005 [24] used a model showing how the *Ap* index and *F10.7* index affect the zonal and meridional wind in the MLT region based data from 1988 to 2000 at 52^{o}N and 2^{o}W. The model was first run without impact of *Ap* and *F10.7*. When these indices were included, a notable change in the 12 hour tide was noted, and also in 6 and 8 hour tides. These results were clearer for the meridional wind. During geomagnetic storms, the meridional wind was found to be perturbed more southwards with a strong dependence. A similar behavior was found for the solar activity, but with a weaker dependence. The zonal wind was found to be perturbed more eastward with more solar activity with a strong dependence, while for geomagnetic activity, the wind seemed to be perturbed more westward with a weak dependence.

In this project, the relationship between meridional and zonal winds in the mid-high latitude NH upper mesosphere and geomagnetic activity along with solar irradiance is investigated using data from eight SuperDARN radars.

4 The Data

4.1 The SuperDARN Radars

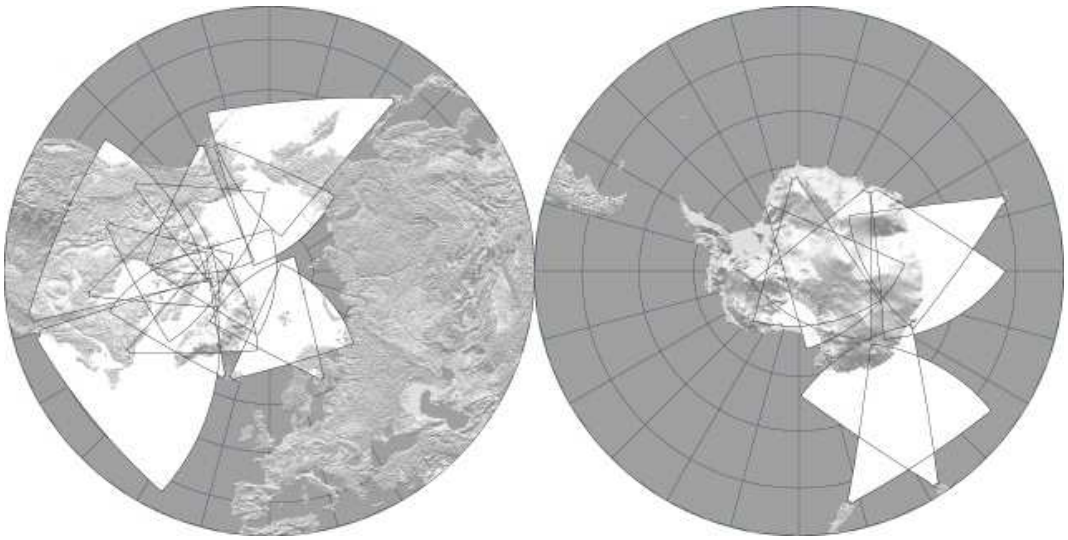

(a) North (b) South

Figure 4: The SuperDARN Radars in a) the northern hemisphere, b) the southern hemisphere [30]

Table 1: Geographic and geomagnetic coordinates for the SuperDarn radars used in this thesis, along with the time span of the data used for each radar [30]. North and east is positive.

Radar	Geographic latitude	Geographic longitude	Geomagnetic latitude	Geomagnetic longitude	Time span [dd.mm.yy]
Goose Bay	53.32	-60.46	61.94	23.02	29.09.93 - 31.08.09
Hankasalmi	62.32	26.61	58.8	105.53	19.06.95 - 31.08.09
Kapuskasing	49.39	-82.32	60.06	-9.22	29.09.93 - 31.08.09
King Salmon	58.68	-156.65	57.43	100.51	04.10.01 - 22.04.09
Kodiak	57.60	-152.2	57.17	96.28	08.01.00 - 18.08.09
Pykkvibær	63.86	-19.20	64.59	69.65	20.11.95 - 31.08.09
Saskatoon	52.16	-106.53	61.34	-45.26	29.09.93 - 31.08.09
Stokkseyri	63.86	-22.02	65.04	67.33	29.08.94 - 04.01.09

The SuperDARN (Super Dual Auroral Radar Network) radars measure the position and Doppler velocity of plasma density irregularities in the Earth's ionosphere. The network consist of 29 radars placed around the polar regions of the Earth, see figure 4. [30]

Hall et al., 1997 [9] showed that the SuperDARN radars could also be used to measure the mesospheric wind. They found that unusual short range (less than 400 km) radar echoes that differed from known irregularities were in fact due to scattering of meteor trails. The Doppler shift from the short range echoes of the

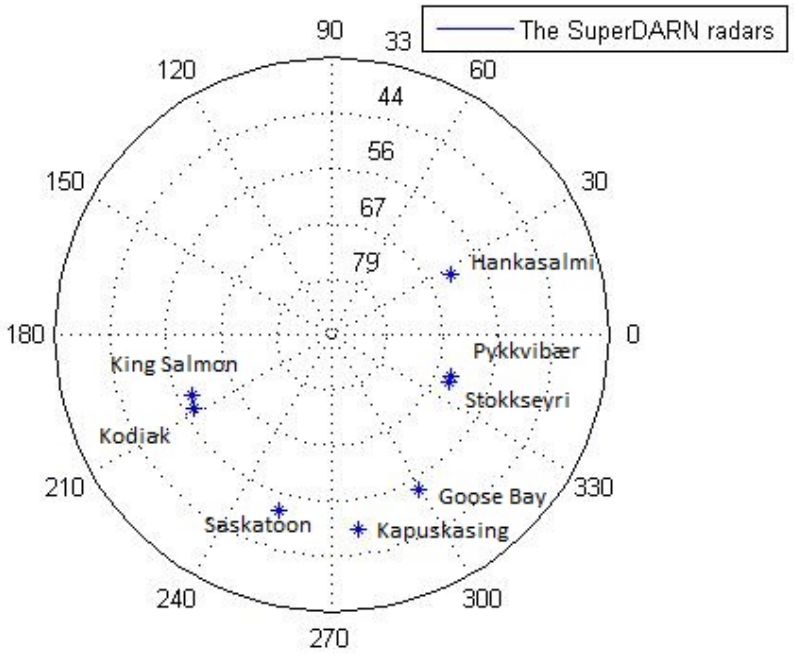

Figure 5: The placement around the north pole of the eight SuperDARN radars used in this thesis.

radar was shown to be consistent with the mesosperic wind measured at the same place by a MF (medium frequency) radar. The height of the measurement was said to be 94 km $\pm$ 3 km.

In this thesis, hourly mean horizontal meteor wind data from the SuperDARN radars Goose Bay, Hankasalmi, Kapuskasing, King Salmon, Kodiak, Pykkvibær, Saskatoon and Stokkseyri obtained from the SuperDARN website [30] have been used. In figure 5, the placement of radars can be seen. The coordinates of the radars are given in table 1 along with the range of the data sets. The radars had a latitudinal span of 14^o and a longitudinal span of 183^o, covering half of the northern hemisphere. The dataset for each radar contain, among other things: A mean meridional wind in m/s where northward wind direction is positive, a mean zonal wind in m/s where westward wind direction is positive, a one sigma standard deviation on the hourly mean fitted meridional wind in m/s and a one sigma standard deviation on the hourly mean fitted zonal wind in m/s. The zonal wind was multiplied by minus one since it is normal convention to use eastward wind as positive.

4.2 The *Ap* Index

The more particles that enter the Earth's ionosphere and magnetosphere, the more the Earth's geomagnetic field is perturbed. This is measured by the K index. The K index is a number from 1 to 9 that isolates how much solar particles affect the geomagnetic field and is an indirect measure of the energy deposited by EPP in the

upper atmosphere [15]. Over a three hour period the maximum deflection of the magnetic field is derived at 13 observatories. The Kp index is the arithmetic mean of the values from the 13 stations, giving a global index for the perturbation of the geomagnetic field. Further, the a index is the linear form of the K index. The relation between the indices are shown in table 6. Finally the Ap index used in this project is the mean a index from all 13 observatories averaged over a day. The Ap index is therefore the linear version of the Kp index. [29]

A monthly Ap index was collected from the web page of the U.S. Dept. of Commerce, NOAA, Space Weather Prediction Center (SWPC) [33] where the observed Ap index was used.

4.3 The *F10.7* Index

The *F10.7* solar radio flux is a measure of solar spectral irradiance emitted in the radio band at a wavelength of 10.7 cm. A global daily value is obtained from Dominion Radio Astrophysical Observatory, Penticton, British Columbia, Canada at local noon. *F10.7* is measured in solar flux units (10^{-22}W m^{-2} Hz^{-1}) [23]. A monthly *F10.7* index was collected from the web page of the U.S. Dept. of Commerce, NOAA, Space Weather Prediction Center (SWPC), where the observed *F10.7* index was used [33].

5 Method

5.1 Preprocessing of the Data

The eight SuperDARN radars used in this thesis started operating between 1993 and 2001 and data until August 2009 have been obtained from most of the radars. They deliver hourly information of the mean meridional and zonal wind, offering great amounts of data. The placement of the radars is shown in figure 5. To be able to investigate the connection between the mesospheric wind and *Ap* and *F10.7*, the data had to be treated in a way that made the comparison as reliable as possible. It was therefore crucial to remove as much of the natural variance as possible. As *Ap* and *F10.7* would not have as much impact on the wind as for instance seasonal effects, it was important to remove these properties that could mask the effects, but without damaging the credibility of the data. Many parameters could increase the variance of the mesospheric wind, for instance geophysical noise, geomagnetic influence, influence from solar activity, seasonal variation and diurnal tides. The solar atmospheric tides and seasonal variability were removed from the monthly mean data as they affect the wind data greatly, and doing so would not remove the credibility of the data remaining. After removing these, a sinusoidal wave was fitted to the remaining wind residuals and a mean monthly perturbation wind was obtained from each fit. This monthly mean wind was then used in the comparison with *Ap* and *F10.7*.

The data preprocessing was done for each radar. Initially, the Hankasalmi radar was used to create a Matlab code that could be applied for all radars. This radar has a long operating time and few data points missing, making it an ideal radar to begin with. In detail the data were first sorted into hours for all months in each year, so that we had a hourly mean month for all years from 1993 to 2009. An example from September, 1996 is shown in figure 6a. To remove the seasonal variety, a monthly mean day was produced from all the years, creating a climatology for each month using data from 1993 to 2009. This can be done assuming the tidal variation in

Table 2: Values for the fitted tide for September 1996 in figure 6c with a 95% confidence interval for the Hankasalmi SuperDARN radar. $Wind$ is the mean residual meridional wind, A_i is the amplitude of the i'th hour component and ϕ_i is the phase displacement of the i'th hour component where $i = 24, 12, 8$.

	Value	$\pm$
$Wind$	-1.5	0.5
A_{24}	-1.0	0.8
A_{12}	-1.7	0.8
A_8	1.2	0.8
ϕ_{24}	0.31	0.12
ϕ_{12}	2.2	0.4
ϕ_8	2.1	0.6

Table 3: Reduction of the variance for the Hankasalmi SuperDARN radar as the data is prepared for comparison with *Ap* and *F10.7*.

	Variance $[m^2/s^2]$
Monthly mean day wind	94
Monthly mean day residual wind	20
Monthly mean residual wind	5.3

the wind is approximately equal for all days in the month. An example is shown in figure 6b. This climatology was then subtracted from all the daily mean months leaving only the residual wind for all monthly plots from 1993 to 2009. The residual solar atmospheric tides with a 24h, 12h and 8h components, as in equation 1, were fitted to these, obtaining the phase and amplitude for the three residual sinusoidals along with the mean residual wind and a confidence interval for all these parameters. These are displayed in table 2. The resultant wind for September 1996 is shown in figure 6c.

Table 3 shows how the variance in the data was reduced after each preprocessing step for the Hankasalmi radar. For the monthly mean day wind in table 3, the variance was taken of the hourly data as used to produce figure 6a for the whole time span of the Hankasalmi radar. For the monthly mean day residual wind, the variance was taken of the hourly data as used to produce figure 6c for the same time span. For the monthly mean residual wind the variance of the mean monthly wind as obtained from the sinusiodal fit in figure 6c was taken for the same time span. Equation 2 was used when finding the variance.

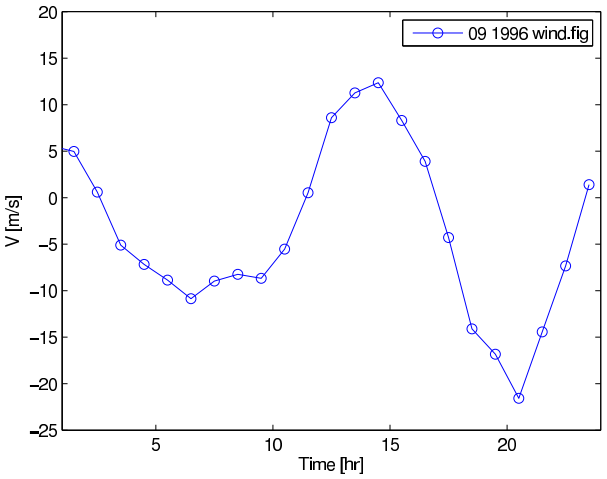

(a) Mean wind for September 1996

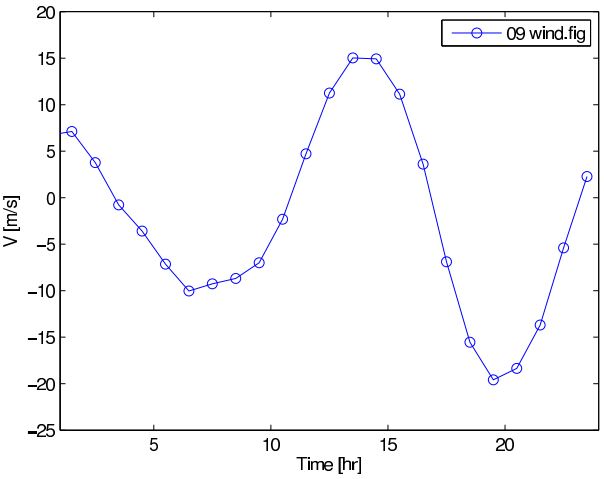

(b) Climatology for September

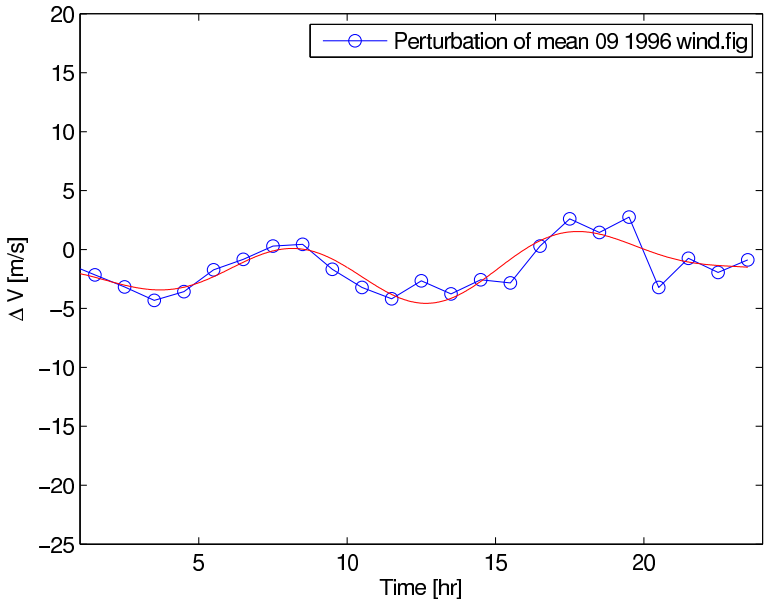

(c) Residual mean wind for September 1996

Figure 6: An illustration of how the seasonal effect on the mesospheric wind was removed, here for September in 1996 for the Hankasalmi SuperDARN radar, meridional wind. Northward is positive. See table 2 for the fitted parameters.

5.2 Data Processing

The next step was to investigate whether there was any connection between the obtained monthly mean residual wind and *Ap*/*F10.7*. The residual winds were used to make correlation plots with the *Ap* and *F10.7* values. A linear regression was performed on the correlation plots to see if there was any statistically significant correlation between them. An example from the Hankasalmi radar is shown in figure 7. The t value from the student's t-test, the correlation coefficient (cc) and the probability of this being a random association, p, was found by using the statistics in appendix A. A two tailed p value was used since there is no a priori knowledge of whether the correlation is negative or positive. The slope of the regression line, a, with boundaries, the cc and the p value can be found in table 7.

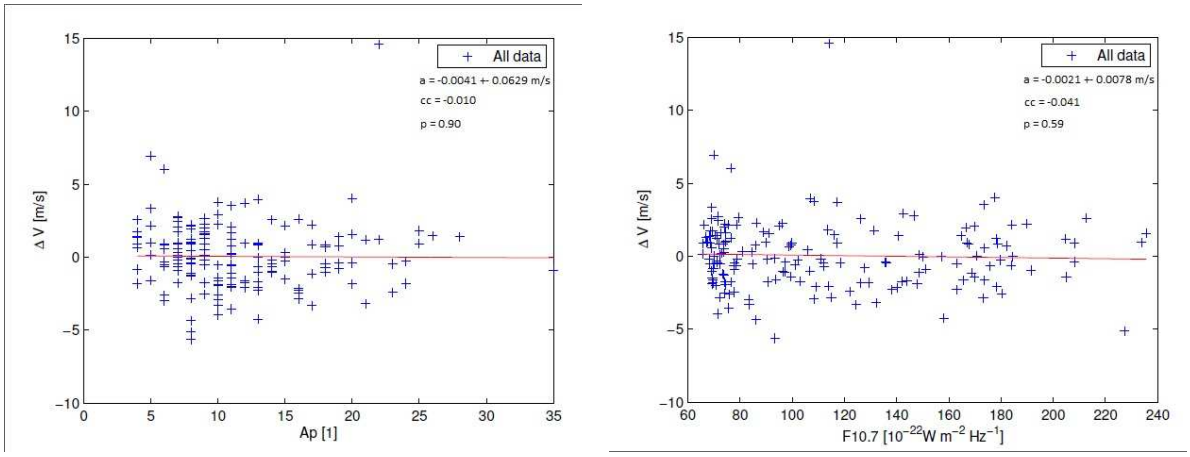

(a) Ap, meridional wind

(b) F10.7, meridional wind

(c) Ap, zonal wind

(d) F10.7, zonal wind

Figure 7: Correlation plots with linear regression for residual meridional/zonal wind vs *Ap/F10.7* using data from the Hankasalmi radar where a is the slope of the regression line, cc is the correlation coefficient and p is the probability of this being a random association using the t-test. n is 171 for all plots and northward and eastward is positive.

As the scatter plots did not show any special features, the residual wind velocities were divided into two groups. One when *Ap/F10.7* was high and one when it was low. To visualize, one can imagine a vertical line placed in the regression plots with one group of wind data of equal size on each side. The wind velocities were divided by finding the highest and lowest *Ap/F10.7* and placing its corresponding wind velocity in its respective group. They were then deleted and new high and low *Ap/F10.7* values could be found, until all had been placed in one of the two groups. A mean was then taken of both groups so that one mean wind velocity at high *Ap/F10.7* and one mean wind velocity at low *Ap/F10.7* was found. These mean winds were then subtracted from one another obtaining a monthly wind perturbation telling in which direction the wind was perturbed by *Ap/F10.7*, and how strong the perturbation was.

To see if the perturbation of the residual wind from *Ap/F10.7* was significant, the perturbation was compared with the square root of the sum of the square of the standard errors of the two points. If the perturbation of the residual wind was larger than the square root of the sum using the one sigma standard error, the perturbation was significant with a 68% confidence level. If it was larger than the sum using the two sigma standard error, the perturbation was significant with a 95% confidence level and larger than the sum using three sigma standard errors gave a 99.7% confidence level. The perturbation with confidence interval of one sigma standard error is shown in table 8.

A polar plot of the wind perturbation from *Ap* and *F10.7* was made as in figure 10 where each radar position is the origin of one wind vector showing the wind perturbation for that radar in polar coordinates. The polar coordinates were obtained from the zonal and meridional wind perturbation, the center of the polar coordinate system was the north pole and the longitudes and latitudes are shown on the axis. This was done to see how the wind moved around the north pole when *Ap/F10.7* was high. The wind perturbation was then used to make bar plots, comparing the geographic and geomagnetic latitudes of the radars with the mean perturbed wind from each radar as in figures 8 and 9.

After doing this for all the data, the same procedure was carried out for the individual months, dividing the residual wind into high and low *Ap/F10.7*, obtaining a wind perturbation for each month to look for seasonal effects on the residual wind. Instead of using the monthly mean wind perturbation directly, the data were smoothed over 3 months. I.e. for February, data from January, February and March were used to find a mean value. This lowered the standard error and could create a more correct image of what happened, as changes in the atmosphere can affect the circulations over several months. An example of the wind perturbation over a year for the Pykkvibær radar is shown in figure 12 where one can see how the wind changes both for *Ap* and *F10.7*.

Contour plots were constructed to look for effects over the months latitudes/longitudes. Both geomagnetic and geographic coordinates were investigated.

Polar plots were made as before, but with one vector for each month at all radar sites, to see how the wind perturbation changed over the months. This was done for *Ap* and *F10.7* using both geographic and geomagnetic coordinates as seen in figure 11. The geomagnetic north pole was set to be at 80.77^{o}N while the longitudinal scale was not changed as this would not alter the result and it would be easier to compare

the two coordinate systems. Data from 2001 were used to place the geomagnetic north pole, a year in the middle of our data timespan [32]. An explanation on how the vector arrows were changed from geographic to the geomagnetic coordinates is presented in appendix B.

Finally, the correlation between *Ap* and *F10.7* was investigated to be able to see if they in fact could be separated at all. Plots of *Ap* and *F10.7* over time were made along with a correlation plot with a linear regression as in figures 14, 15 and 16.

6 Results and Discussion

Figure 8 a, shows the perturbation in residual meridional wind from *Ap* and *F10.7* for the eight radars plotted according to their geographic latitude. We see that the perturbed wind appears to be more northward with increasing latitudes. When investigating further by fitting a line, y=ax+b, to this, using weighted data, it is revealed that the slope, a, is different from 0 with a confidence level of 95% for none of the slopes. The slopes and confidence bounds can be seen in table 4. For zonal wind in 8 b, it is not as easy to see any connections, but for high *F10.7* the wind tends to be more westward with increasing latitude although this is not statistically significant.

In figure 9, the wind perturbation from *Ap* for the eight radars plotted according to their geomagnetic latitude is shown. As the solar particles enter the atmosphere in the auroral oval with its center in the geomagnetic north pole, geomagnetic coordinates are more appropriate to use when investigating effects from these. It can be seen that a clearer tendency for more northward and eastward wind perturbation at high *Ap* as the geomagnetic latitude increases. Singer et al., 1994 [28] found enhanced westward directed winds when *Ap* was high, at middle geomagnetic latitudes (50-55^{o}N) and enhanced eastward directed winds when *Ap* was high, at high geomagnetic latitudes (60.5^{o}N). Although the highest latitudes of Singer et al., 1994 are middle latitudes in this project and the significance of their result is not the best, the movement of the wind from westward to eastward with higher geomagnetic latitude coincides well with figure 9, where the zonal wind, when *Ap* is high, seems to move more eastward with higher latitude. The slope crosses the x-axis at 58.3^{o}N for the zonal wind, coinciding well with Singer's results having a change in direction of the zonal wind between 55^{o}N and 60.5^{o}N. The data from the linear regression can be found in table 4. The increasingly eastward/northward wind perturbation with increasing latitude can also mainly be seen in the zonal wind, both in figure 8 and 9. Singer et al., 1994 found a smaller effect in the meridional wind than in the zonal wind which has also been found in this work, as the zonal wind perturbation often is twice the magnitude of the meridional wind perturbation. This could cause a latitudinal effect in the meridional wind, if any, to be more difficult to distinguish.

Table 4: Slopes of the regression lines seen in figure 8 and 9 and their 95% confidence limits for residual wind perturbation from *Ap*/*F10.7* and meridional/zonal wind vs geographic and geomagnetic latitude. Northward and eastward is positive.

	Geographic latitude. Slope [m/s]	Geomagnetic latitude. Slope [m/s]
F10.7 meridional wind	0.048 ± 0.091	-
F10.7 zonal wind	-0.10 ± 0.12	-
Ap meridional wind	0.043 ± 0.064	0.051 ± 0.11
Ap zonal wind	-0.0038 ± 0.16	0.19 ± 0.25

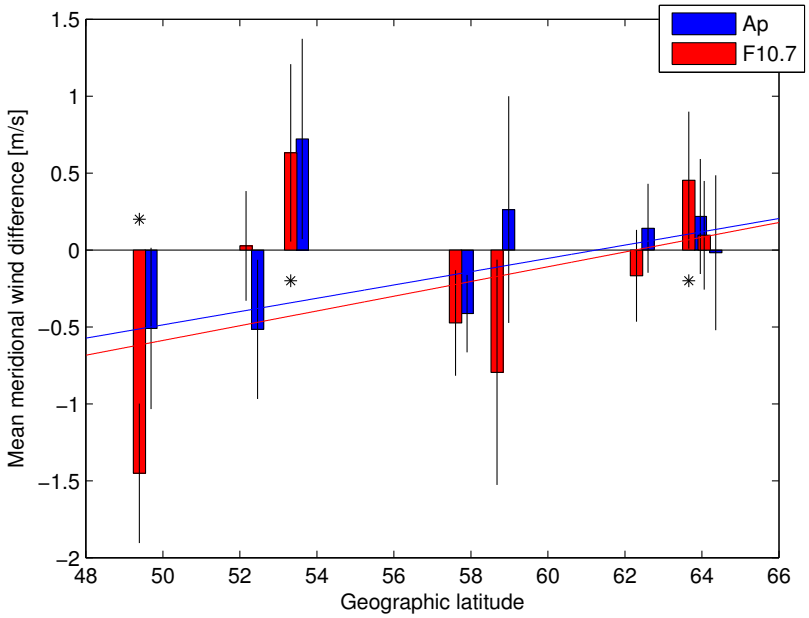

(a) Meridional wind

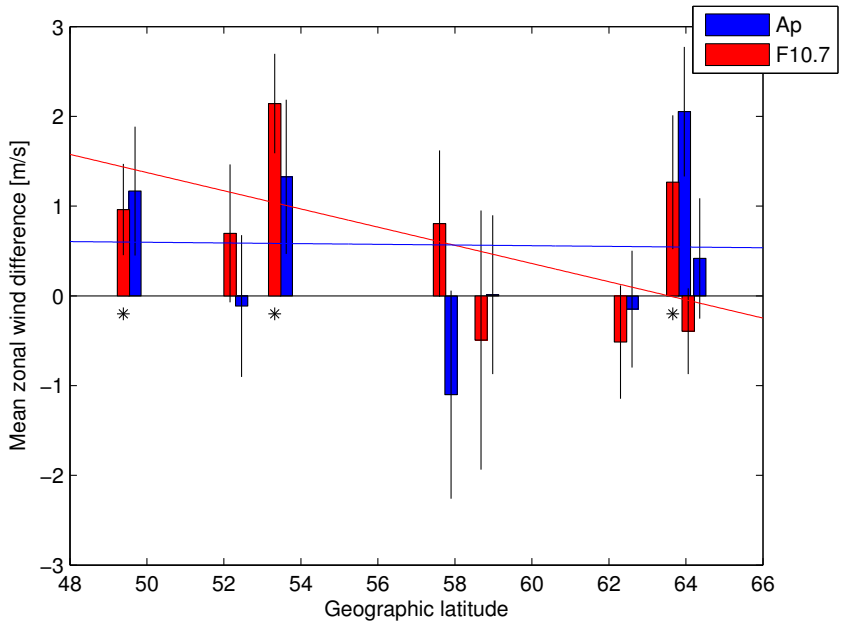

(b) Zonal wind

Figure 8: The perturbation in residual wind from *Ap*/*F10.7* plotted against geographic latitude. A mean meridional wind perturbation for eight SuperDARN radars was found from *Ap* and *F10.7* in (a), where the *Ap* data are blue and the *F10.7* data are red. A linear fit is also added for each. The same is found for the zonal wind in (b). The radars are represented by their respective placement in latitudes as presented in table 1. The errorbars are the one sigma standard error and the three significant radars seen in figure 10 are indicated with black stars. Northward and eastward is positive.

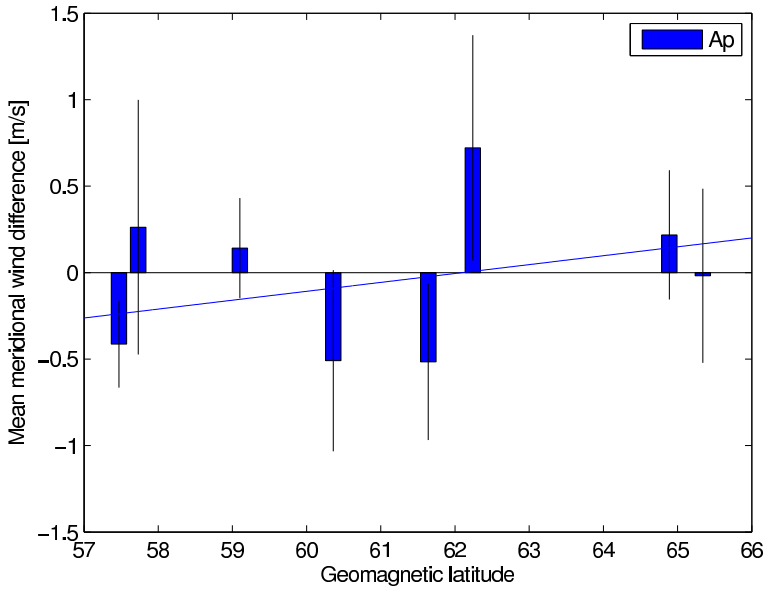

(a) Meridional wind

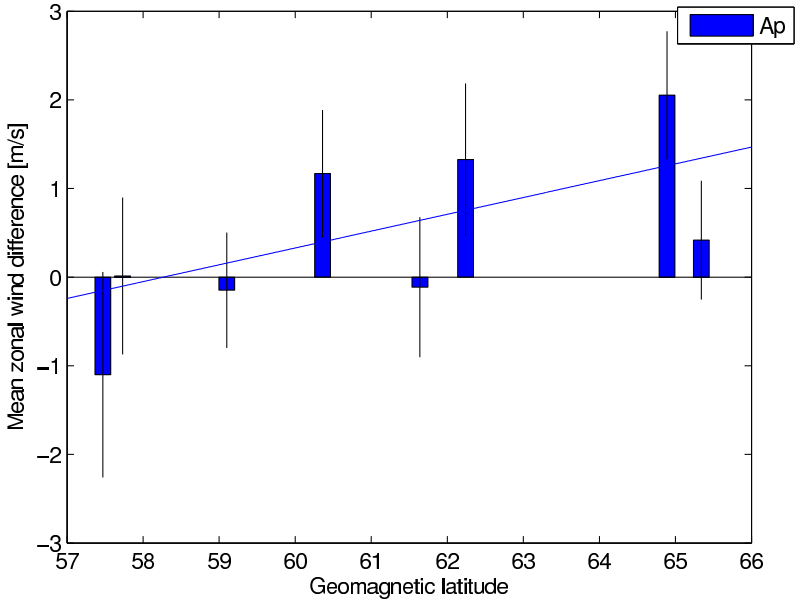

(b) Zonal wind

Figure 9: The perturbation of the residual wind from *Ap* plotted against geomagnetic latitude. A mean meridional wind perturbation for eight SuperDARN radars was found from *Ap* in (a). A linear fit is also added for each. The same is found for the zonal wind in (b). The radars are represented by their respective placement in latitudes as presented in table 1. The errorbars are the one sigma standard error and northward and eastward is positive.

Pancheva et al., 2005 [24], by use of an empirical model based on data at 52^oN and 2^oW, found a strong equatorward perturbation by geomagnetic activity and the same effect, but weaker, for solar activity. For zonal winds, a strong eastward perturbation by solar activity was found and the geomagnetic activity was found to perturb the zonal wind in a westward direction. By looking at the Saskatoon radar in figure 8 (the second from the left) in this thesis, which is at a similar latitude (53^oN) as that used of Pancheva et al., 2005, the same effects can be seen except for solar influence on the meridional wind. The result for *F10.7* meridional wind at this latitude both in this thesis and for Pancheva et al., 2005 were however weak, and in the latter, below the 68% significance threshold.

In figure 8 and 9, the one sigma standard error is used for the error bars, meaning that the significance of the data points is quite low. The wind perturbation for each radar was found by taking the mean of all months in a year. As these varied in direction for each month, as seen in figure 12, the resultant mean wind over a year is rather small, and has a high standard error.

In figure 10, a polar plot of all radars with the yearly mean perturbation of residual wind from *Ap*/*F10.7* is shown, where the thick lines are the significant ones with one sigma standard error. Here, the radars Pykkvibær, Goose Bay and Kapuskasing stands out as the significant ones both for *Ap* and *F10.7*. The wind perturbation appears to be equatorward and eastward for all significant radars.

Polar plots were also made for the monthly mean for all radars. This was done both for *Ap* and *F10.7* in geographic and geomagnetic coordinates as displayed in figure 11. This was done mainly to see if there was any obvious difference in how the wind behaved around the geomagnetic and geographic north pole. The wind perturbation tends to be equatorward, especially for *Ap*, indicating a connection between the wind and both the *Ap* and *F10.7* index.

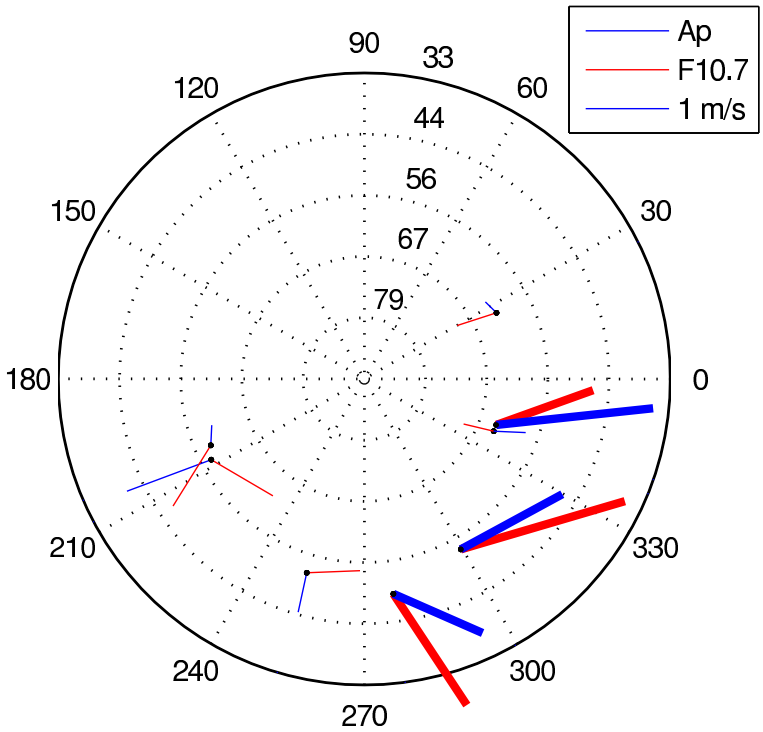

Figure 10: A polar plot of the perturbation of the residual wind from *Ap*/*F10.7* in geographic coordinates. A mean wind perturbation for each radar was found for *Ap* and *F10.7*, where the *Ap* data are blue and the *F10.7* data are red. The significant data above one sigma standard error are plotted with thick lines. The length of the vector arrows is indicated in the box, and the vectors spring out from the placement of the eight SuperDarn radars, represented by black dots. These radars are presented in table 1.

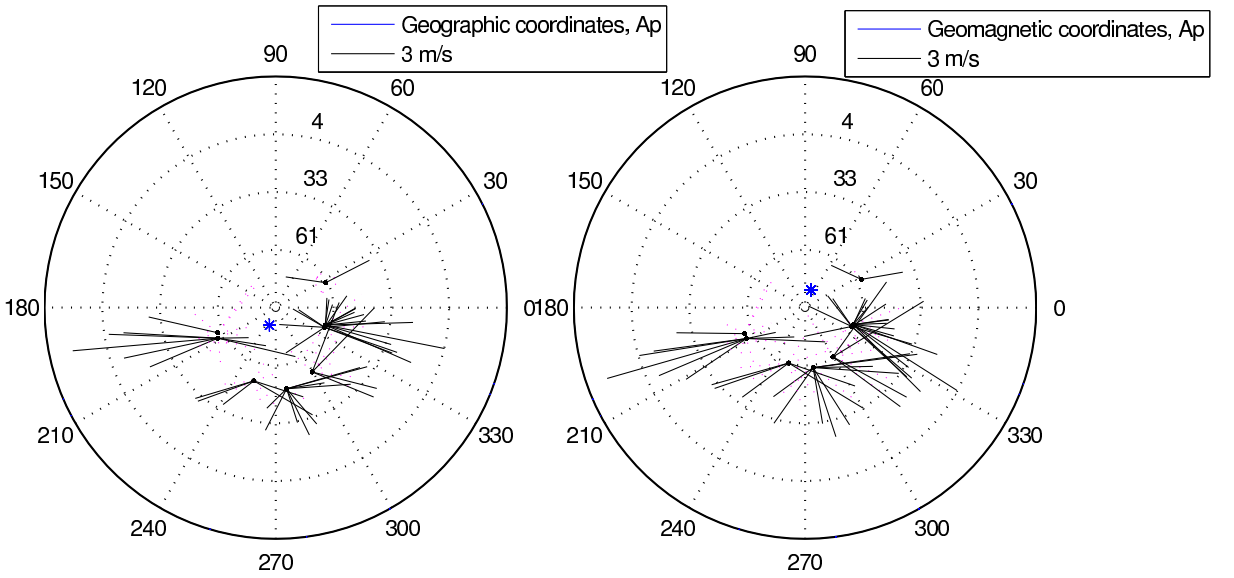

(a) Geographic coordinates, Ap

(b) Geomagnetic coordinates, Ap

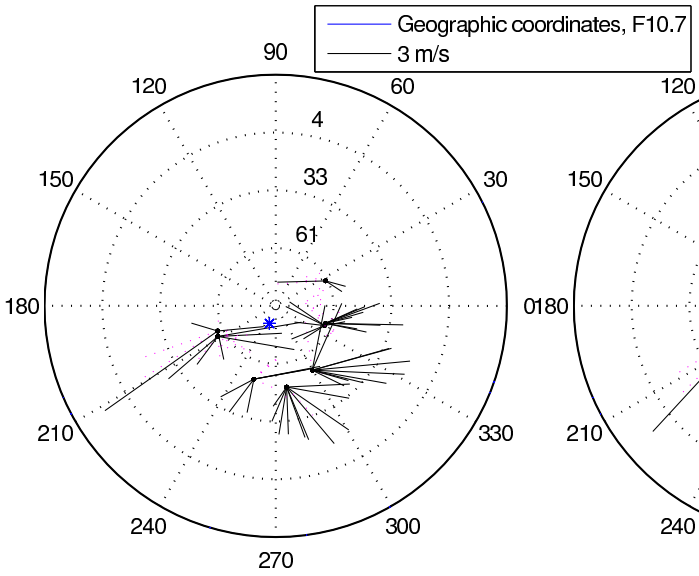

(c) Geographic coordinates, F10.7

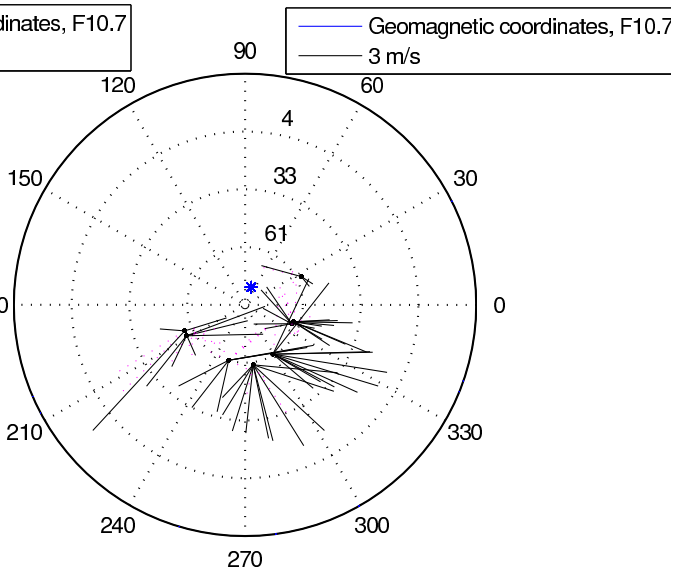

(d) Geomagnetic coordinates, F10.7

Figure 11: Polar plots of the monthly mean residual wind perturbations. Only the significant wind perturbations within a two sigma standard error are shown. The blue star is the north pole in the other coordinate system and the black dots show the location of the SuperDARN radars.

The mean wind perturbation of *Ap* and *F10.7* over all radars and all months is stated in table 5. The zonal mean zonal perturbation is significant both for *Ap* and *F10.7*, and shows similar properties though the perturbation is somewhat stronger from *F10.7* with a basically equal standard error. The perturbation is insignificantly southward and significantly eastward for both *Ap* and *F10.7*. This was also found by Pancheva et al., 2005 [24] as further discussed above, except for perturbation in the meridional wind from the *F10.7* index. Their findings were however only based on one radar.

Lu et al.,2007 [14] found more westward winds in the stratosphere with increasing geomagnetic activity, which is the opposite of what is found in this thesis. Since the stratosphere has an opposite wind behavior than that of the mesosphere due to the selective filtering of gravity waves, the wind could be perturbed in an eastward way in the mesosphere leading to a westward wind in the stratosphere as this information is propagated downwards with the gravity waves.

In figure 10 one can see that the Pykkvibær, Goose Bay and Kapuskasing radars have a significant wind perturbation from both *Ap* and *F10.7*. It would therefore be natural to look at one of these radars at higher temporal resolution. A plot of the monthly mean wind perturbation from both *Ap* and *F10.7* for the Pykkvibær radar can be seen in figure 12 where the error bars are the one sigma standard error. The data for *Ap* are plotted in red and for *F10.7* in blue. The green line is the perturbation from *Ap* for the Stokkseyri radar, close to the Pykkvibær radar both in longitude and latitude. Figures of the perturbation of the residual wind for Goose Bay and Kapuskasing is displayed in figure **??** and **??** in appendix C. The perturbation in residual wind for the Pykkvibær radar varies over a year. In winter the zonal wind is significantly perturbed eastwards though the magnitude of the perturbation is smaller outside the winter months and in summer the signal is insignificant. The meridional wind is perturbed northwards most of the year by high *Ap* with southward perturbation in winter. For *F10.7* it varies more, but is mainly northward. When looking at the plots for the other radars both for meridional and zonal wind, it was found that the way the wind is perturbed when *Ap*/*F10.7* is high during a mean year, varies from radar to radar. When comparing the plots according to where they were placed in longitude, no consistent picture of the wind perturbation could be found. Radars placed close together however, (Stokkseyri and Pykkvibær, King Salmon and Kodiak) often had similar behavior. This strengthens the results as radars with different time span and properties display similar results. Similar results were also found from the Kodiak and King Salmon radars which are located close to each other.

Table 5: Mean perturbation of residual meridional/zonal wind from *Ap*/*F10.7* with the one sigma standard error from all radars over all months. Northward and eastward is positive.

	Mean perturbation of residual wind [m/s]
Ap, meridional	-0.014 ± 0.16
Ap, zonal	0.45 ± 0.36
F10.7, meridional	-0.21 ± 0.24
F10.7, zonal	0.56 ± 0.34

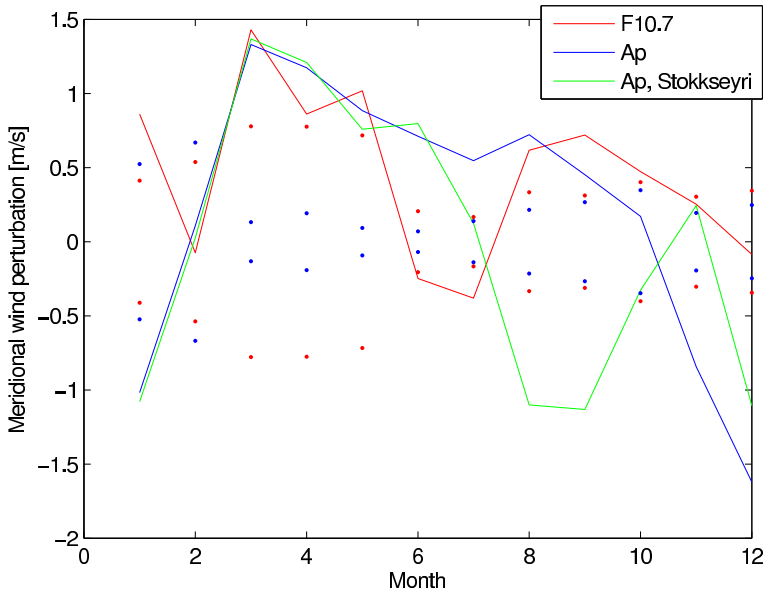

(a) Meridional wind

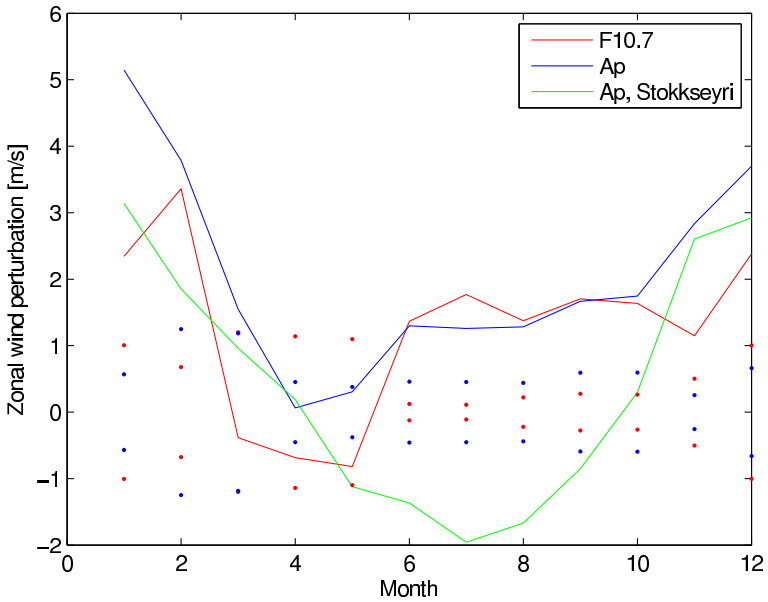

(b) Zonal wind

Figure 12: The wind perturbation from *Ap* and *F10.7* for the Pykkvibær SuperDARN radar for a monthly mean year, where the *Ap* data are shown in blue and the data for *F10.7* are presented in red. The wind perturbation from *Ap* for the Stokkseyri SuperDARN radar is added in green. The error bars are the one sigma standard error also color coded as mentioned above for the Pykkvibær radar. Northward and eastward is positive.

The perturbation of the residual wind from *Ap* and *F10.7* is similar in figure 12 as the curves follow each other quite consistently. This was also the case for many of the other radars. When looking at the same type of plots for all the radars, similar plots could mainly be seen for the same latitudes both for *Ap* and *F10.7*, zonal and meridional wind. This is illustrated in a contour plot as in figure 13. It appears that *Ap* and *F10.7* affect the wind in a similar manner over the latitudes and months. However, a stronger southward wind perturbation is seen for *F10.7* than for *Ap* for meridional wind expanding further north. For zonal wind the effect is also similar for *Ap* and *F10.7*, but a stronger westward wind perturbation is seen for *F10.7*, breaking up the positive perturbation seen for *Ap* at mid-latitudes in winter and spring. In the zonal wind, a negative perturbation can be seen in winter and spring while positive is seen in summer and autumn for both *Ap* and *F10.7* . For meridional wind there is a positive trend in winter and autumn, and a negative trend in spring and summer. The areas of strongest wind perturbation are significant both for *Ap* and *F10.7* with a two sigma standard error.

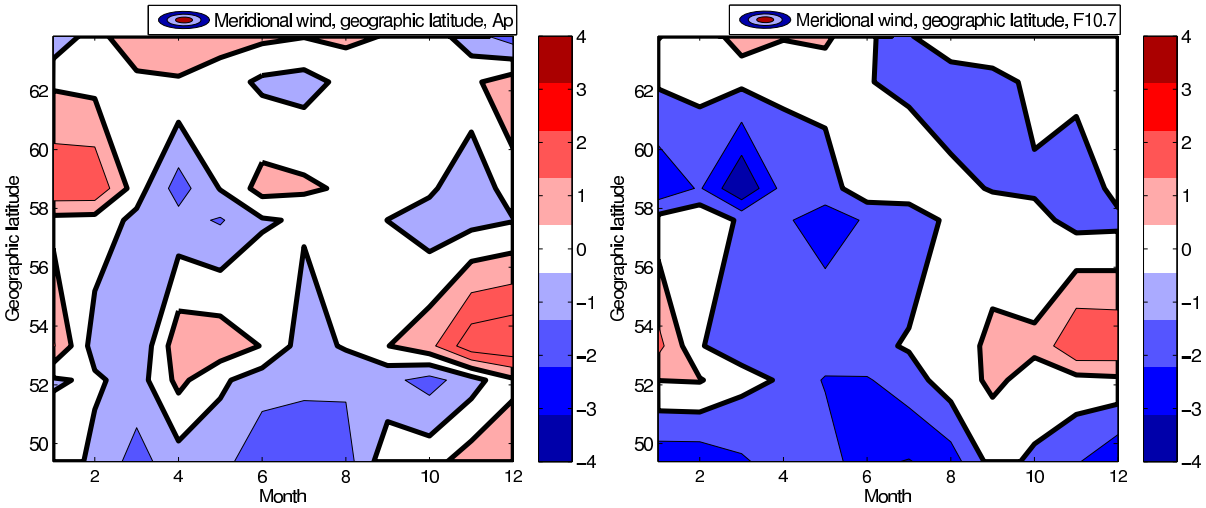

(a) Meridional wind, Ap

(b) Meridional wind, F10.7

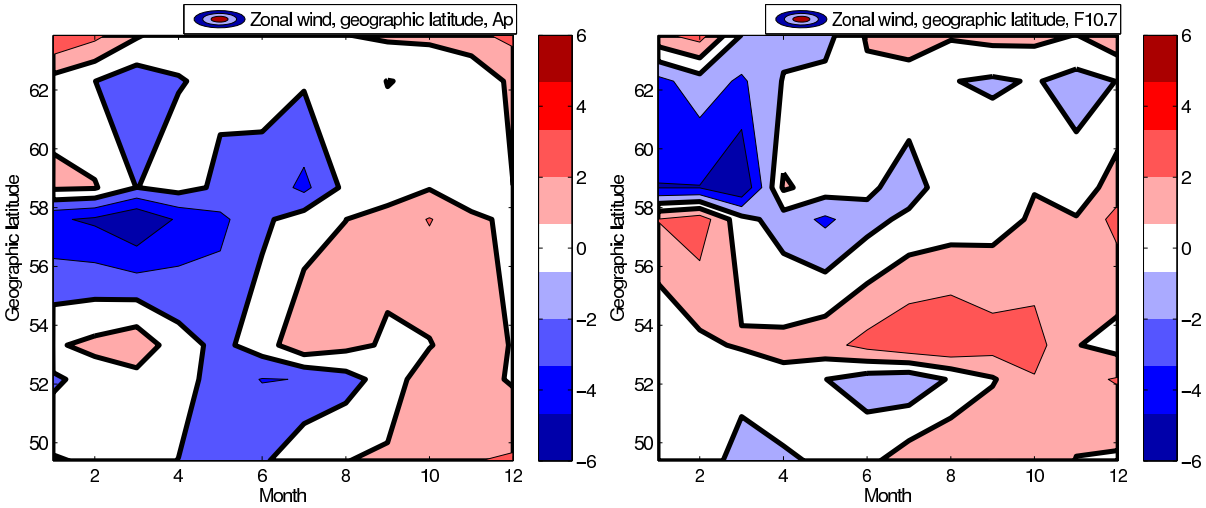

(c) Zonal wind, Ap

(d) Zonal wind, F10.7

Figure 13: Contour plots of the wind perturbation between high and low *Ap* and *F10.7* for meridional and zonal wind for months vs geographic latitude. Northward and eastward is positive.

Keuer et al., 2007 [11] investigated wind perturbation due to solar irradiance for various heights at 54.6^{o}N and 13.4^{o}E. The SuperDARN radars obtain their information around 94 km [9], and only the results for over 85 km was interesting to compare with this thesis. Above 85 km Keuer et al., 2007 found an eastward perturbation by solar irradiance in summer and a westward perturbation in winter for the zonal wind. In figure 13d, a somewhat similar effect can be seen at 54.5^{o}N, but the wind perturbation is mainly eastward all year although close to zero in the winter months. In summer/autumn the strongest eastward perturbation for this latitude can be seen. For the meridional wind, Keuer et al., 2007 found equatorward perturbation both in summer and winter. In figure 13b in this thesis, a northward perturbation is found in early winter and an equatorial perturbation in early summer at the same latitude.

Ap has its peak when *F10.7* is in the descending phase and it is often assumed that they are not very closely correlated on long time scales. When investigating this further by plotting them against each other, a correlation coefficient of 0.46 was found showing a medium correlation when using the the same time span as for the Pykkvibær radar, see figures 14, 15 and 16. *Ap* and *F10.7* are closely related for small values, typically seen around solar minimum. When *Ap* and *F10.7* increase, so does the spread around the regression line showing little correlation for large values. When looking at how many months have both the *Ap* and *F10.7* indices above its respective median value, 47 months were found to have both indices above the mean. 83 months had both indices below the mean and 36 months had either high *Ap* and low *F10.7* or high *F10.7* and low *Ap*. To be able to distinguish the effect the indices have on the mesospheric wind, the months where one was high and the other low must be investigated in more detail with a more sophisticated analysis.

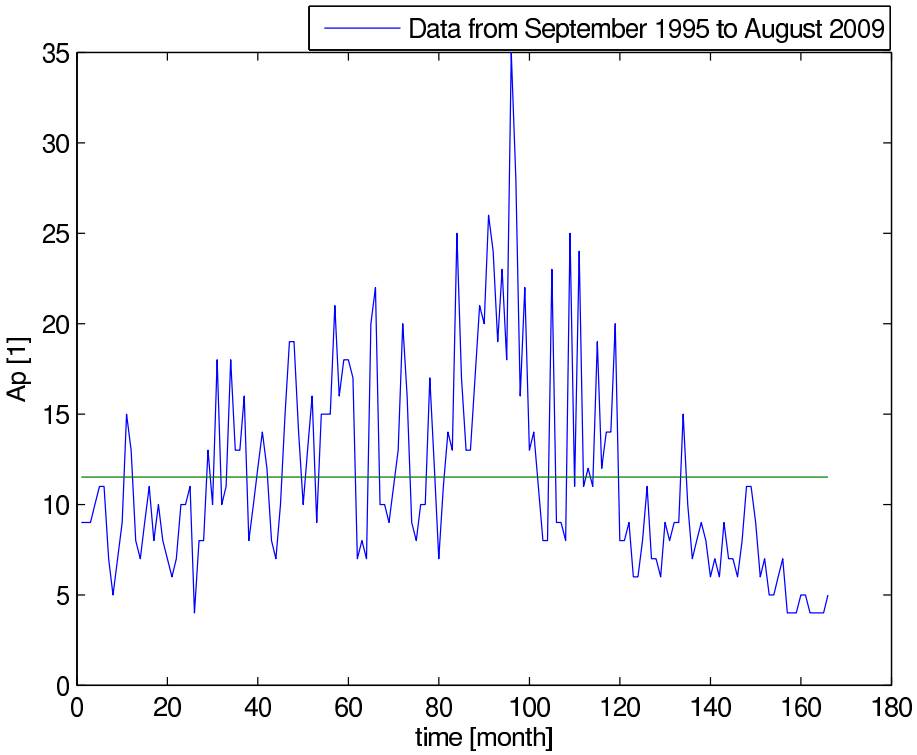

Figure 14: Change in the *Ap* index over time.

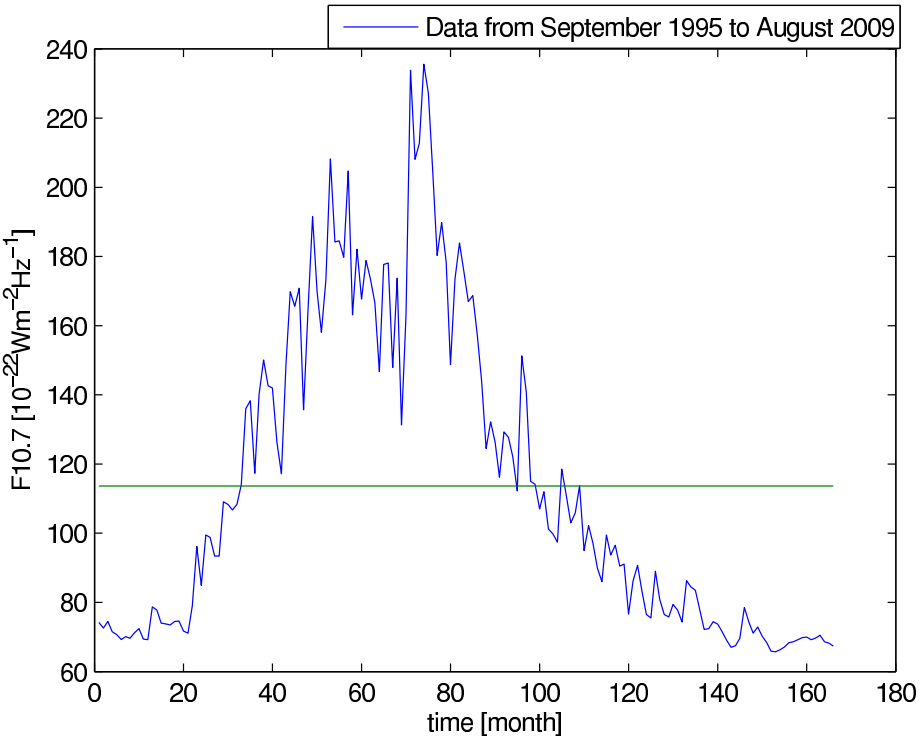

Figure 15: Change in the *F10.7* index over time.

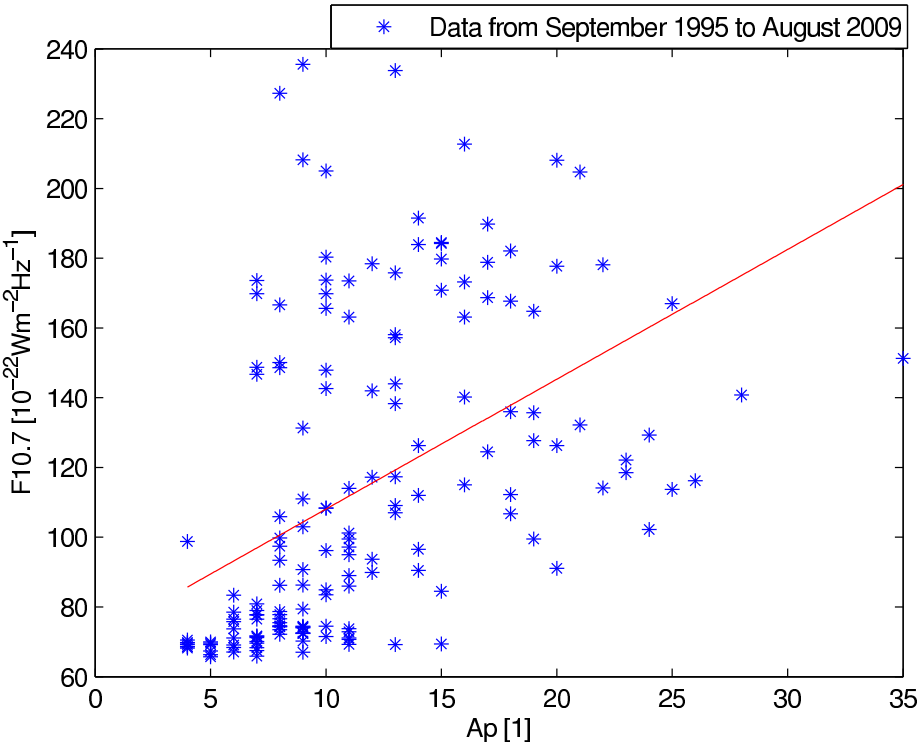

Figure 16: Correlation plot with linear regression for *Ap* vs *F10.7*. The slope of the regression line, a, is 3.7 ± 1.1 10^{-22}W m^{-2} Hz^{-1} with a 95% confidence interval and the correlation coefficient, cc, is 0.46.

7 Conclusion

Either the solar radiance or the solar particles entering the Earth's atmosphere appear to affect the mesospheric circulation by driving the winds southward and eastward. Some of the effect might come from perturbations of the wind further up in the atmosphere and some from EPP directly increasing the NO_x content and ozone depletion in the mesosphere. These effects have been shown to be able to move down to the stratosphere with the planetary waves in winter, affecting the circulation significantly. When looking at *Ap* and *F10.7* the perturbation of the wind had a tendency for being equatorward and eastwards when looking at polar plots for geomagnetic and geographic coordinates using monthly data, and the effect was more evident for *Ap*.

There was some evidence for a latitudinal connection where *Ap* perturbed the wind more eastward with increasing latitudes when looking at geomagnetic coordinates. This was also found by Singer et al., 1994 [28]. The zonal wind was also more perturbed than the meridional wind also noted by Singer et al, 1994.

Three radars had statistically significant perturbation for the wind vector summing zonal and meridional wind components both for *Ap* and *F10.7*. They showed a tendency towards eastward and southward perturbation. This was also found when taking the mean of all radars. The meridional southward perturbation was insignificant both for *Ap* and *F10.7*, but the zonal eastward perturbation was significant for both parameters, and with a slightly higher perturbation for *F10.7*.

The results were strengthened of the fact that radars at similar sites showed similar behavior and Keuer et al., 2007 [11] and Pancheva et al., 2005 [24] found similar perturbations of the wind at similar latitudes as in this thesis.

As the wind perturbation has seasonal variability, it is better to use the monthly values than taking the mean over a year as the perturbation becomes much smaller and the standard error increase. The data from Pykkvibær, Goose Bay and Kapuskasing gave significant perturbation when using the mean over a year, one could therefore look at one of these radars in more detail. The Hankasalmi and King Salmon radars showed few significant wind perturbations.

When looking at the solar effect on the mesosphere, both *Ap* and *F10.7* can be used as parameters and will show a similar result. It is not possible to say that one is better than the other, because when they showed different results one did not stand out as the parameter that perturbed the wind less or the one with smaller standard error. The analysis made here was not sufficiently advanced to differentiate the effect of *Ap* and *F10.7* over the time period that the radars were recording data, but some tendencies were found.

Further work could include a similar study of the SH, as there are also SuperDARN radars functioning there. One could also look at how Ap and F10.7 affect the mesosphere when they enter and why they affect it so similarly. A more advanced analysis of the data focusing on the months where the *Ap* was high and the *F10.7* was low or vice versa should be performed to differentiate their effects on the mesospheric wind.

References

[1] Andrews, David G., An Introduction to Atmospheric Physics, second edition, Pages 8, 12-14, 128-136, Cambridge University Press, 2010

[2] Arnold, N. F., Robinson, T. R., Solar magnetic flux influences on the dynamics of the winter middle atmosphere, Geophysical Research Letters, Volume 28(12), Pages 2381-2384, doi:10.1029/2000GL012825, 2001

[3] Baldwin, M. P., Gray, L. J., Dunkerton, T. J., Hamilton, K., Haynes, P. H., Randel, W. J., Holton, J. R., Alexander, M. J., Hirota, I., Horinouchi, T., Jones, D. B. A., Kinnersley, J. S., Marquardt, C., Sato, K., Takahashi, M., The Quasi-Biennal Oscillation, Reviews of Geophysics, Volume 39, pages 179-229, 1999RG000073, 2001

[4] Baumgaertner, A. J. G., McDonald, A. J., Fraser, G. J., Plank, G. E., Long-term observations of mean winds and tides in the upper mesosphere and lower thermosphere above Scott Base, Antarctica. Journal of Atmospheric and Solar-Terrestrial Physics, Volume 67, Pages 1480-1496, doi:10.1016/j.jastp.2005.07.018, 2005

[5] Brasseur, G., Solomon, S., Aeronomy of the middle atmosphere, second edition, D. Reidel Publishing Company, Boston, 1986

[6] Chang, L. C., Thayer, J. P., Lei, J., Palo, S. E., Isolation of the global MLT thermal response to recurrent geomagnetic activity, Geophysical Research Letters, Volume 36, L15813, DOI:10.1029/2009GL039305, 2009

[7] Daae, M., Espy, P., Sarays, F., Newnham, D., The effect of radiation belt particles on middle atmospheric night time ozone during enhanced geomagnetic activity, Presentation number A071S4_7PM1. Thursday, 7 July 2011 1330-1500 MR208 IAGA-A071S4_1399, International Union of Geodesy and Geophysics (IUGG) General Assembly, Melbourne Australia, 28 June 2011 - 7 July 2011

[8] Espy, P. J., Lecture 2 - Overview of the Atmosphere, Lecture notes FY3201 Atmospheric Physics, 2011

[9] Hall, G. E., MacDougall, J. W., Moorcroft, D. R., St. Maurice, J. P., Manson, A. H., Meek, C. E., Super Dual Auroral Radar Network observations of meteor echoes, Journal of Geophysical Research, Volume 102, Pages 14603-14614, doi:10.1029/97JA00517, 1997

[10] Holton, J. R., Alexander, M. J., The role of waves in the transport circulation of the middle atmosphere, in Atmospheric Science Across the Stratopause, Geophysical Monograph Series, Volume 123, edited by D. E. Siskind, S. D. Eckermann, and M. E. Summers, Pages 21-35, doi:10.1029/GM123p0021, AGU, Washington, D. C., 2000

[11] Keuer, D., Hoffmann, P., Singer, W., and Bremer, J., Long-term variations of the mesospheric wind field at mid-latitudes, Annales Geophysicae, Volume 25, pages 1779-1790, doi:10.5194/angeo-25-1779-2007, 2007.

[12] Lei, J., Thayer, J. P., Forbes, J. M., Sutton, E. K., Nerem, R. S., Rotating solar coronal holes and periodic modulation of the upper atmosphere, Geophysical Research Letters, Volume 35, L10109, doi:10.1029/2008GL033875, 2008a

[13] Lei, J., Thayer, J. P., Forbes, J. M., Sutton, E. K., Nerem, R. S., Temmer, M., Veronig, A. M., Global thermospheric density variations caused by high-speed solar wind streams during the declining phase of solar cycle 23, Journal of Geophysical Research , Volume 113, A11303, doi:10.1029/2008JA013433, 2008b

[14] Lu, H., Jarvis, M. J., Graf, H. F., Young, P. C., Horne, R. B., Atmospheric temperature responses to solar irradiance and geomagnetic activity, Journal of Geophysical Research, Volume 112, D11109, doi:10.1029/2006JD007864, 2007

[15] Lu, H., Clilverd, M. A., Seppala, A., Hood, L. L., Geomagnetic perturbations on stratospheric circulation in late winter and spring, Journal of Geophysical Research, Volume 113, D16106, DOI: 10.1029/2007JD008915, 2008

[16] NASA, Earth's Inconstant Magnetic Field,

http://www.nasa.gov/vision/earth/lookingatearth/29dec_magneticfield.html, 2012

[17] NASA, Goddard Space Flight Center,

http://www.nasa.gov/centers/goddard/news/topstory/2003/0313irradiance.html, 2012

[18] NASA, Marshall Space Flight Center, Solar Physics, The Sunspot Cycle, http://solarscience.msfc.nasa.gov/SunspotCycle.shtml, 2012

[19] NASA, Solar Cycle Primer,

http://www.nasa.gov/mission_pages/sunearth/news/solarcycle-primer.html, 2012

[20] NASA, Solar System,

http://www.nasa.gov/topics/solarsystem/features/sun-brightness.html, 2012

[21] Newnham, D. A., Espy, P. J., Clilverd, M. A., Rodger, C. J., Seppälä, A., Maxfield, D. J., Hartogh, P., Holmén, K., Horne, R. B., Direct observations of nitric oxide produced by energetic electron precipitation into the Antarctic middle atmosphere, Geophysical Research Letters, Volume 38, L20104, doi:10.1029/2011GL048666, 2011

[22] NOAA, Wandering of the geomagnetic Poles,

http://www.ngdc.noaa.gov/geomag/GeomagneticPoles.shtml, 2012

[23] NorthWest Research Associates, INC. Space Weather Services, 10.7cm Solar Radio Flux, http://www.nwra.com/spawx/f10.html, 2012

[24] Pancheva, D., Mukhtarov, P., Mitchell, N. J. and Muller, H. G., Empirical model of the dynamics in the mesosphere and lower thermosphere region over the UK, including solar and geomagnetic activity, Journal of Atmospheric and Solar-Terrestrial Physics, Volume 67, No. 1-2, pages 197-209, doi:10.1016/j.jastp.2004.07.0292005, 2005

[25] Pogoreltsev, A. I., Vlasov, A. A., Fröhlich, K., Jacobi, C., Planetary waves in coupling the lower and upper atmosphere, Journal of Atmospheric and Solar-Terrestrial Physics, Volume 69, doi:10.1016/j.jastp.2007.05.014, 2007

[26] Raman, K. S., Space Weather - Sun Earth Relations, International Journal of Astronomy and Astrophysics, Volume 01, No. 01, Pages 10-14, doi:10.4236/ijaa.2011.11003, 2011

[27] Rottmann, K., Matematisk formelsamling, 11. edition, Page 40, Spektrum forlag, 2010

[28] Singer, W., Bremer, J., Hoffmann, P., Manson, A. H., Meek, C. E., Schminder, R., Kurschner, D., Portnyagin, Yu. I., Makarov, N. A,. Muller, H. G., Kazimirovsky, E. S., Clark, R. R., Geomagnetic influences upon tides-winds from MLT radars, Journal of Atmospheric and Terrestrial Physics, Volume 56, No. 10 , pages 1301-1311, 1994

[29] Space Physics Interactive Data Resource (SPIDR),

Geomagnetic And Solar Indices Data Description,

http://spidr.ngdc.noaa.gov/spidr/help.do?group=geomInd#ap, 2011

[30] Super Dual Auroral Radar Network (SuperDARN),

http://superdarn.jhuapl.edu/index.html, 2011

[31] Thayer, J. P., Lei, J., Forbes, J. M., Sutton, E. K., Nerem, R. S., Thermospheric density oscillations due to periodic solar wind high-speed streams, Journal of Geophysical Research, Volume 113, A06307, doi:10.1029/2008JA013190, 2008

[32] U.S. Dept. of Commerce, NOAA, Geomagnetic Data of the North Pole, http://www.ngdc.noaa.gov/geomag/data/poles/NP.xy, 2012

[33] U.S. Dept. of Commerce, NOAA, Space Weather Prediction Center (SWPC), Recent Solar Indices of Observed Monthly Mean Values, http://www.swpc.noaa.gov/ftpdir/weekly/RecentIndices.txt, 2011

[34] Walpole, R. E., Myers, R. H., Myers, S. L., Ye, K., Probability and Statistics for Engineers and Scientists, eight edition, Pages 121, 280, 402-403, Prentice Hall, 2007

[35] http://easycalculation.com/statistics/p-value-t-test.php, 2011

[36] http://www.atmosp.physics.utoronto.ca/people/loic/chemistry.html, 2012

[37] http://www.daviddarling.info/encyclopedia/A/atmospheric_window.html, 2012

A Statistics

The variance of a sample can be found with the equation

$$\sigma^2 = \frac{1}{n-1}\sum_{i=1}^{n}(x_i - \bar{x})^2 \tag{2}$$

where n is the number of elements in the sample. The standard deviation σ is the square root of the variance.

The mean standard deviation, σ_m, of a sample with n known standard deviations can be found with:

$$\sigma_m = \sqrt{\frac{\sum_{i=1}^{n}\sigma_i^2}{n}}. \tag{3}$$

When adding or subtracting two sets of sample data with known standard deviation, the new standard deviation, σ, is found with the equation

$$\sigma = \sqrt{\sigma_1^2 + \sigma_2^2}. \tag{4}$$

The standard error, $std.e$, of a sample of size n with standard deviation σ, can be found with the equation

$$std.e = \frac{\sigma}{\sqrt{n}}. \tag{5}$$

Using equation 3 for σ_{m_1} and σ_{m_2} in equation 4, gives a σ_m from the mean of two samples when the data points of the samples are added or subtracted. A $std.e$ for this can be found with equation 5. If the samples have the same size n, this gives:

$$std.e = \frac{\sigma_m}{\sqrt{n}} = \frac{\sqrt{\sigma_{m_1}^2 + \sigma_{m_2}^2}}{\sqrt{n}} = \sqrt{std.e_1^2 + std.e_2^2} \tag{6}$$

where $std.e_1$ and $std.e_2$ are the standard errors of each sample.

To find the sample correlation coefficient (cc) between the samples A and B, the equation

$$cc = \frac{\sum_m \sum_n (A_{mn} - \bar{A})(B_{mn} - \bar{B})}{\sqrt{[\sum_m \sum_n (A_{mn} - \bar{A})^2][\sum_m \sum_n (B_{mn} - \bar{B})^2]}} \tag{7}$$

can be used where $\bar{A}$ and $\bar{B}$ are the mean of the samples A and B respectively. This gives a number between -1 and 1 where 0 means no correlation.

If a linear correlation between the samples is assumed, a correlation plot with a linear regression, $y = ax + b$, can be made. The distance between a data point and the regression line in the direction of the y-axis is called a residual, ϵ. From the linear regression plot, the sum of squares of residuals (SSE),

$$\text{SSE} = \sum_{i=1}^{n}\epsilon_i^2, \tag{8}$$

and the gradient of the regression line a can be found.

The most common method to investigate if the correlation is significant is the students t test. The students t test can be used as a test of whether the slope of a regression line differs significantly from 0. SSE and a is used to find the t value with the equation:

$$t = \frac{(a - a_0)\sqrt{n-2}}{\sqrt{\text{SSE}/\sum_{i=1}^{n}(A_i - \bar{A})^2}} \tag{9}$$

where A is on the x-axis. Here a_0 is the number from which we want to see if the line differs significantly, in this case 0 and n-2 are the degrees of freedom where n is the number of data points in the samples.

A p value, showing the probability of the correlation being a random association, can be found using t distribution tables, Microsoft Office Excel, or an interactive calculating web page. The Matlab function corr() has also been used. It must be considered if the distribution is two-tailed or one-tailed. [34]

B Coordinate Conversion

This explanation is based on figure 17. With any triangle the sine sentence [27]

$$\frac{a}{sinA} = \frac{b}{sinB} = \frac{c}{sinC} \tag{10}$$

can be used where a, b and c are the sides of the triangle and A, B and C are the opposite angles. By using equation 10 in figure 17 one can see that

$$\frac{magnlat}{sinb} = \frac{r}{sina}, \tag{11}$$

where r is the distance between the magnetic north pole, indicated by the blue cross, and the geographic north pole in degrees of latitude, [32](data from 2001), *magnlat* is the distance in degrees of latitude, from the geomagnetic north pole to the point where the radar is in geomagnetic coordinates. The angle between the blue and green line is 109.48 minus the absolute value of the geographic longitude as the angle from 0 to the green line is 109.48 degrees (The known longitudinal change when changing the coordinate system from geographic to geomagnetic, [32](data from 2001)) and the angle between 0 and the blue line is the absolute value of the geographic longitude coordinate of the relevant radar. The length of the blue line is not known as it could be longer or shorter than the distance from the geographic north pole to the radar in geographic coordinates, but this does not affect the geometrics used. The angle a which should be obtained is the needed change of angle of the vector arrows as one goes from one coordinate system to another. Note: An arrow which goes through the geomagnetic north pole when looking at geomagnetic coordinates, should also go through the geomagnetic north pole when looking at geographic coordinates even though the coordinate system has been changed.

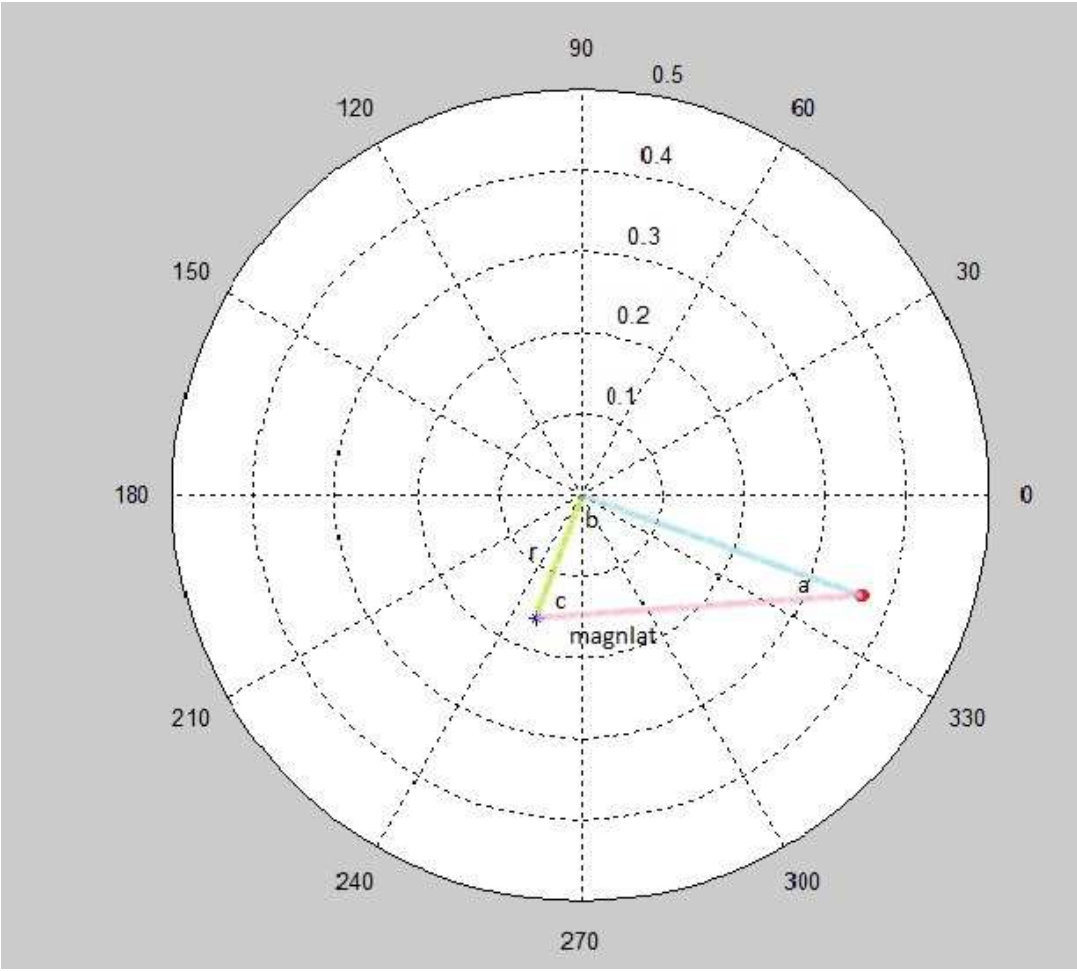

Figure 17: How the vectors were changed from geographic coordinates to geomagnetic coordinates.

C Tables

Table 6: Relation between the K index and a index

K [1]	0	1	2	3	4	5	6	7	8	9
a [1]	0	3	7	15	27	48	80	140	240	400

Table 7: Slopes of regression line with a 95% confidence interval, cc and p value of the linear fit of meridional/zonal residual wind and *Ap*/*F10.7* as in figure 7 for all SuperDARN radars used in this thesis. Northward and eastward is positive.

Radar	*Ap* meridional wind, slope of regr. line [m/s]	*Ap*, mer *cc*	*Ap*, mer *p*	*Ap* zonal wind, slope of regr. line [m/s]	*Ap*, zon *cc*	*Ap*, zon *p*
Goose Bay	0.038 ± 0.105	0.053	0.48	0.17 ± 0.17	0.15	0.048
Hankasalmi	-0.0041 ± 0.0629	-0.010	0.90	-0.022 ± 0.121	-0.027	0.72
Kapuskasing	-0.085 ± 0.062	-0.20	0.0082	0.074 ± 0.123	0.088	0.23
King Salmon	-0.022 ± 0.130	-0.036	0.74	0.038 ± 0.215	0.037	0.73
Kodiak	-0.043 ± 0.058	-0.14	0.15	-0.082 ± 0.107	-0.14	0.13
Pykkvibær	0.047 ± 0.062	0.12	0.13	0.15 ± 0.12	0.20	0.0109
Saskatoon	-0.039 ± 0.061	-0.092	0.21	0.015 ± 0.113	0.018	0.80
Stokkseyri	0.016 ± 0.089	0.027	0.73	0.039 ± 0.107	0.055	0.47
Radar	*F10.7* meridional wind, slope of regr. line [m/s]	*F10.7*, mer *cc*	*F10.7*, mer *p*	*F10.7* zonal wind, slope of regr. line [m/s]	*F10.7*, zon *cc*	*F10.7*, zon *p*
Goose Bay	0.013 ± 0.013	0.15	0.0425	0.016 ± 0.021	0.11	0.15
Hankasalmi	-0.0021 ± 0.0078	-0.041	0.59	0.020 ± 0.015	0.021	0.79
Kapuskasing	-0.019 ± 0.008	-0.32	8.6e-6	0.0088 ± 0.0168	0.076	0.30
King Salmon	-0.025 ± 0.020	-0.26	0.013	-0.029 ± 0.033	-0.18	0.087
Kodiak	-0.0060 ± 0.0075	-0.15	0.12	0.011 ± 0.014	0.14	0.14
Pykkvibær	0.0049 ± 0.0077	0.097	0.21	0.0072 ± 0.0148	0.075	0.34
Saskatoon	-0.00070 ± 0.00820	-0.012	0.87	0.0077 ± 0.0152	0.073	0.32
Stokkseyri	-0.0028 ± 0.0052	-0.039	0.61	-0.0037 ± 0.0131	-0.042	0.58

Table 8: Meridional/zonal residual wind perturbation by *Ap*/*F10.7* with the one sigma standard error for all SuperDARN radars used in this thesis. Northward and eastward is positive.

Radar	*Ap*,mer wind, perturbation [m/s]	*Ap*, zon wind perturbation [m/s]	*F10.7*, mer wind perturbation [m/s]	*F10.7*, zon wind perturbation [m/s]
Goose Bay	-0.71 ± 0.57	-1.6 ± 0.9	-1.3 ± 0.6	-2.1 ± 0.9
Hankasalmi	0.36 ± 0.35	0.24 ± 0.67	0.11 ± 0.35	0.20 ± 0.67
Kapuskasing	0.82 ± 0.37	-0.61 ± 0.72	1.6 ± 0.4	-1.3 ± 0.7
King Salmon	1.4 ± 0.8	1.6 ± 1.4	0.30 ± 0.83	0.93 ± 1.38
Kodiak	0.40 ± 0.36	1.1 ± 0.7	0.58 ± 0.36	-0.26 ± 0.68
Pykkvibær	-0.39 ± 0.35	-1.8 ± 0.7	2.4 ± 0.6	2.4 ± 0.6
Saskatoon	0.58 ± 0.35	0.37 ± 0.66	-0.062 ± 0.357	-0.73 ± 0.66
Stokkseyri	0.035 ± 0.484	-0.31 ± 0.58	0.19 ± 0.48	0.26 ± 0.58